Journal of Computational Physics 484 (2023) 112083

Contents lists available at ScienceDirect

Journal of Computational Physics

journal homepage: www.elsevier.com/locate/jcp

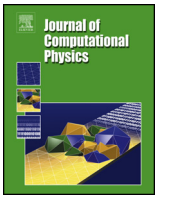

Accessibility constraints in structural optimization via distance functions

Grégoire Allaire [a,*], Martin Bihr [b], Beniamin Bogosel [a], Matias Godoy [a]

[a] CMAP, CNRS, École polytechnique, Institut Polytechnique de Paris, 91120 Palaiseau, France
[b] Safran Tech, Rue des jeunes Bois, 78117 Chateaufort, France

ARTICLE INFO

Article history:
Received 22 November 2022
Received in revised form 16 March 2023
Accepted 16 March 2023
Available online 29 March 2023

Keywords:
Topology optimization
Additive manufacturing
Support
Accessibility
Level set

ABSTRACT

This paper is concerned with a geometric constraint, the so-called accessibility constraint, for shape and topology optimization of structures built by additive manufacturing. The motivation comes from the use of sacrificial supports to maintain a structure, submitted to intense thermal residual stresses during its building process. Once the building stage is finished, the supports are no longer useful and should be removed. However, such a removal can be very difficult or even impossible if the supports are hidden deep inside the complex geometry of the structure. A rule of thumb for evaluating the ease of support removal is to ask that the contact zone between the structure and its supports can be accessed from the exterior by a straight line which does not cross another part of the structure. It mimicks the possibility to cut the head of the supports attached to the structure with some cutting tool. The present work gives a new mathematical way to evaluate such an accessibility constraint, which is based on distance functions, solutions of eikonal equations. The main advantage is the possibility of computing shape derivatives of such a criterion with respect to both the structure and the support. We numerically demonstrate in 2D and 3D that, in the context of the level-set method for topology optimization, such an approach allows us to optimize simultaneously the mechanical performance of a structure and the accessibility of its building supports, guaranteeing its manufacturability.

© 2023 Elsevier Inc. All rights reserved.

This work is dedicated to the memory of Roland Glowinski, who was a pioneer in many aspects of computational mathematics. In particular, he published in the early eighties one of the first numerical computation of what is known today as the homogenization method for topology optimization of structures [20].

1. Introduction

Manufacturability constraints are very important in structural optimization to ensure that the resulting optimal designs are realistic and not just proofs of concept which turn out to be infeasible in industrial practice. Very often these manufacturability constraints are translated in geometric constraints like, for example, minimal or maximal thickness, uniform smoothness of the boundary, feature size or imposed molding direction. There is a rich literature on the topic and we refer to [22], [21], [38], [23], [7], [6] and references therein. Additive manufacturing, which is a key technology for building

* Corresponding author.
E-mail address: gregoire.allaire@polytechnique.fr (G. Allaire).

https://doi.org/10.1016/j.jcp.2023.112083
0021-9991/© 2023 Elsevier Inc. All rights reserved.

complex optimal structures obtained by topology optimization [32], [27], has its own limitations which induce new manufacturability constraints. These constraints are mostly due to the high and unevenly distributed temperatures, generated by the laser beam, melting the metallic powder. The temperature gradients induce thermal residual stresses or thermal dilations of the printed structure. This phenomenon is primarily observed on structures which have large portions of surfaces which are close to being horizontal (in case of a vertical build direction). Such horizontal regions are called overhangs. A typical additive manufacturing constraint in topology optimization is to penalize such overhangs [4], [15], [28], [29], [31].

However, in some cases it is not possible to avoid overhang regions and therefore, to build the structure, it is necessary to add so-called support parts which mitigate these deformation effects due to the building process. Once the fabrication is finished, these supports are removed, which can be a tricky post-processing operation. In particular, to remove the supports with a cutting tool, one should be able to access the surface where the supports are attached to the built structure. One possible way to evaluate this accessibility is to check if a straight line, not crossing the structure, can be drawn from the attachment surface to the outside of the build chamber or computational domain. If one such straight line cannot be found, it is sure that some region of the manufactured part obstructs the passage of the cutting tool to reach some region of the attachment surface, whatever position it takes from the outside. Of course, this straight line cannot touch the built structure but it can lie either in the void region or in the support region since the supports can be progressively cropped from the outside. Clearly, this criterion is a first-order approximation since one can argue that curved tools can be operated or that, rather than a straight line, a small cylinder should be guaranteed for the cutting tool to access the contact surface. Nevertheless, we believe this criterion is already a key preliminary step in the assessment of support accessibility.

The goal of the present work is to give a proper mathematical definition of this accessibility constraint which is amenable to optimization. In doing so, we shall replace the above intuitive geometrical description by a more convenient criterion which is evaluated in terms of distance functions. The use of distance functions to evaluate geometrical objective functions is not new and already appeared in several works including [6], [7], [40]. A first consequence of relying on distance functions is that the resulting criterion can be easily discretized and thus numerically evaluated. A second, and more important, consequence is that such a criterion can be differentiated with respect either to the shape of the built structure (which plays the role of an obstacle) or to the shape of the supports (which can choose their attachment zone with the built structure). There were already a few studies on this accessibility problem. In [41] the shape of the supports is optimized using the SIMP method for an accessibility problem. In [33] the shape of a structure is optimized in order for its boundary to be machinable. Finally, our previous work [1] already introduced a similar accessibility criterion, which was evaluated by a ray tracing algorithm, but was intrinsically not optimizable. Therefore, our main original contribution is to propose a new differentiable accessibility criterion which is easily inserted in a topology optimization algorithm.

For simplicity, in a first step, we ignore the motivation from additive manufacturing and even any mechanical equations: in a purely geometrical setting we introduce two definitions of accessibility for any space dimension, 2D or 3D. This is done in Section 2 where the goal is to determine if a target surface Γ_{out} is accessible from a starting surface Γ_D in the sense that any point on Γ_{out} can be connected to Γ_D by a straight line which does not intersect an obstacle Ω_-. The first and more general definition, called multi-directional accessibility, puts no restriction on the direction of this straight line and evaluates a discrete version of this accessibility criterion through the computation of distance functions. The second and more restrictive definition, called normal accessibility, requires that the connecting straight line is normal to the starting surface Γ_D. Such a definition is more demanding and less often verified but it has the advantage of requiring only one distance function evaluation and thus is numerically cheaper. A last ingredient for evaluating these two accessibility criteria is a penalization method for the obstacle when solving the eikonal equation, the solution of which is the required distance function. More precisely, the obstacle is filled with an ersatz material with a smaller propagation speed, compared to that outside from the obstacle.

Section 3 introduces the objective functions which are going to be used in optimization problems in order to enforce admissibility. These objective functions are least-square criteria comparing distance functions with and without obstacles. They are always non-negative and they vanish in case of accessibility. Section 4 establishes shape derivatives for the proposed accessibility criteria with respect to the shape of the obstacle. Section 5 does the same for shape derivatives with respect to the target surface. Our approach heavily relies on the penalized version of the eikonal equations. In truth our analysis is mostly formal because the proposed adjoint equation is a conservative transport equation, featuring a non-smooth advection velocity. Thus, existence and uniqueness of the adjoint is not obvious although our numerical results seem to indicate it is indeed well-posed.

Section 6 recalls the classical problem in structural optimization of compliance minimization with a volume constraint. Furthermore, we propose an approach to couple it with an accessibility constraint. Section 7 describes the numerical algorithms used for the test cases which are presented in the remaining sections. Section 8 focuses on purely geometrical examples, while Section 9 describes mechanical examples. First, a 2D cantilever is optimized for compliance minimization with an accessibility constraint. Secondly, a 3D application to additive manufacturing is considered. The problem is to simultaneously optimize a structure (a bridge) for its final use and its supports for guaranteeing its fabrication. Furthermore, since the supports must be removed at the end of the manufacturing process, an accessibility constraint is added in order to improve the ease of removal. We conclude this paper with some perspectives and open problems in Section 10.

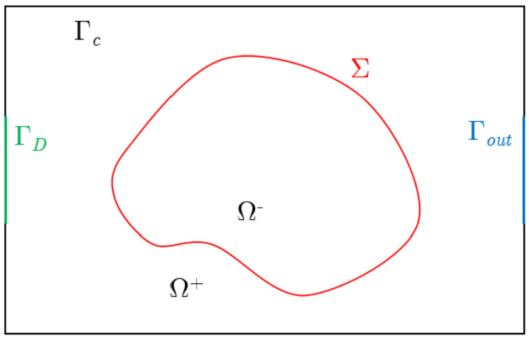

Fig. 1. Domain Ω split in two subdomains by an interface Σ.

2. Two definitions of accessibility

Let $\Omega \subset \mathbb{R}^d$ ($d = 2$ or 3 in practice) be a bounded open set, which is assumed to be convex and smooth enough (say, with a Lipschitz boundary). It is divided in two sub-domains Ω_- and Ω_+, separated by an interface Σ (a surface), such that $\Omega = \Omega_+ \cup \Sigma \cup \Omega_-$. The role of Ω_- is to be an obstacle, while Ω_+ is the free space around it. For simplicity, it is assumed that Ω_- is strictly included in Ω, in other words its boundary coincides with the interface Σ which is a closed surface inside Ω (see Fig. 1). The boundary of the whole domain Ω is divided in three disjoint components, $\partial\Omega = \Gamma_D \cup \Gamma_c \cup \Gamma_{\rm out}$, where $\Gamma_{\rm out}$ is the subset of $\partial\Omega$ which has to be accessible from another subset Γ_D. Finally, $\Gamma_c = \partial\Omega \setminus (\Gamma_D \cup \Gamma_{\rm out})$ is the rest of the boundary. It is assumed that neither $\Gamma_{\rm out}$ nor Γ_D are empty (more precisely, both have non-vanishing surface measure). Fig. 1 shows the different subdomains and boundaries of Ω.

The goal of this section is to define a mathematical notion of accessibility to the **target surface** $\Gamma_{\rm out}$ from the **starting surface** Γ_D, which is amenable to numerical computation and optimization. In loose terms, accessibility means that each point on $\Gamma_{\rm out}$ must be connected to a point on Γ_D by a straight line, which does not cross the obstacle Ω_-. In the sequel, two such definitions of accessibility are introduced, which rely on different families of straight lines. The first one is the most general one and is called **multi-directional accessibility**: any straight line is admissible, whatever its orientation. The second definition is more restrictive (but turns out to be easier to check) and is called **normal accessibility**: only those straight lines which are normal to the starting surface Γ_D are admissible.

2.1. Multi-directional accessibility

Let us start by giving the first definition of **multi-directional accessibility**. A point $x \in \Gamma_{\rm out}$ is multi-directionally accessible from Γ_D if there exists a point $y \in \Gamma_D$ such that the segment $[xy]$ is contained in Ω_+ and does not intersect the obstacle Ω_- (see the right picture in Fig. 2). To quantify this definition, we introduce the geodesic distance in Ω_+

$$L_\Sigma(x, y) = \inf\{l(\gamma) \text{ with } \gamma(t) : [0, 1] \to \Omega_+, \gamma(0) = x, \gamma(1) = y\}, \tag{1}$$

where $l(\gamma)$ is the length of the curve γ inside Ω_+. Then, the fact that $[xy]$ is contained in Ω_+ (and does not cross Ω_-) is equivalent to the equality $L_\Sigma(x, y) = |x - y|$. In other words, the distance circumventing the obstacle is the usual euclidean distance. Indeed, it is always true that $L_\Sigma(x, y) \geq |x - y|$ and equality holds if and only if the segment $[xy]$ (which is the shortest path between x and y, in the absence of obstacle, since Ω is assumed convex) is contained in Ω_+. This definition was first introduced in [1] where accessibility was evaluated but not optimized. One novelty of the present work is that we devise a method to improve accessibility by optimizing the shape of the obstacle.

Let us explain how the distance $L_\Sigma(x, y)$ was numerically computed in our previous work [1], relying on a ray-tracing algorithm. The starting surface Γ_D is discretized by a collection of points y_i, $1 \leq i \leq N_y$, the target surface $\Gamma_{\rm out}$ is discretized by points x_j, $1 \leq j \leq N_x$, and we simply checked if the rays $[x_j y_i]$ intersect or not the obstacle. Such an algorithm is very simple but is not amenable to differentiation with respect to the shape of the obstacle or of the target surface.

Therefore, to make this definition easily computable and optimizable, we propose a different discretization, relying on distance functions which are computed as solutions of eikonal equations. The first step is, as before, to discretize the starting surface Γ_D by N_y points y_i. The second step is to fix a small parameter $\epsilon > 0$ and to introduce small balls $\mathcal{B}_{y_i}$ of radius ϵ and center y_i. The signed distance function d_{y_i} from $\mathcal{B}_{y_i}$ is computed in $\Omega_+ \setminus \mathcal{B}_{y_i}$ by solving the eikonal equation

$$\left\{ \begin{array}{rcl} |\nabla d_{y_i}(x)| & = & 1 \quad \text{in } \Omega_+ \setminus \mathcal{B}_{y_i}, \\ d_{y_i} & = & 0 \quad \text{on } \partial\mathcal{B}_{y_i}. \end{array} \right. \tag{2}$$

It should be compared to the signed distance function $d_{0,y_i}(x)$ from $\mathcal{B}_{y_i}$ in the complete domain (without the obstacle), which is a solution of another eikonal equation

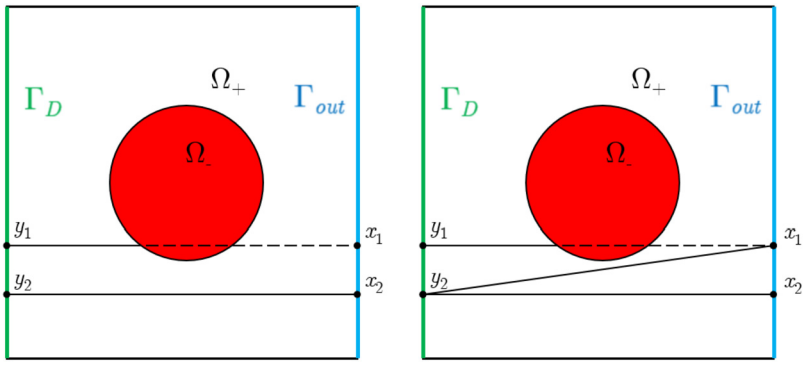

Fig. 2. Normal accessibility (left): x_2 is normally accessible but not x_1. Multi-directional accessibility (right): both x_2 and x_1 are multi-directionally accessible from the same y_2.

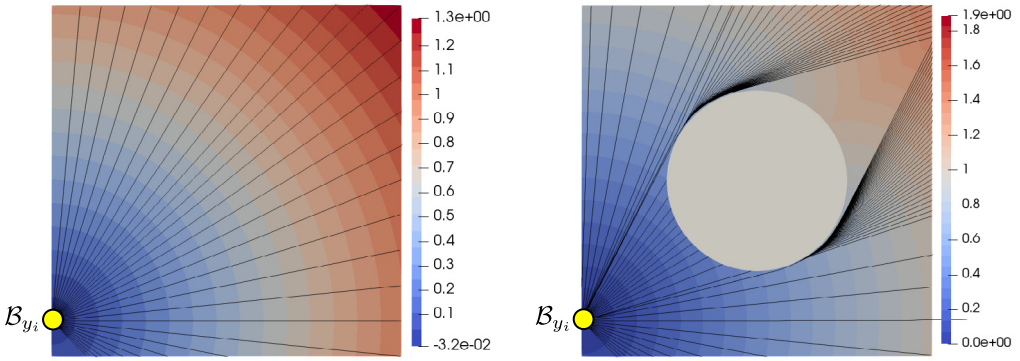

Fig. 3. Streamlines or rays of d_{0,y_i} (left, without obstacle) and d_{y_i} (right, with obstacle) issued from the yellow ball $\mathcal{B}_{y_i}$. (For interpretation of the colors in the figure(s), the reader is referred to the web version of this article.)

$$\begin{cases} |\nabla d_{0,y_i}(x)| &= 1 \quad \text{in } \Omega \setminus \mathcal{B}_{y_i}, \\ d_{0,y_i} &= 0 \quad \text{on } \partial\mathcal{B}_{y_i}. \end{cases} \tag{3}$$

Of course, for any $x \in \Gamma_{\text{out}}$, one has that $d_{y_i}(x) \geq d_{0,y_i}(x)$. The case of equality, for at least one index i, gives rise to our first accessibility definition.

Definition 2.1 *(Multi-directional accessibility).* Fix a family of points $y_i \in \Gamma_D$, $1 \leq i \leq N_y$ and a small radius $\epsilon > 0$. A point $x \in \Gamma_{\text{out}}$ is multi-directionally accessible from Γ_D if there exists at least one point $y_i \in \Gamma_D$ such that $d_{y_i}(x) = d_{0,y_i}(x)$.

The surface Γ_{out} is multi-directionally accessible from Γ_D if any point $x \in \Gamma_{\text{out}}$ is multi-directionally accessible from Γ_D.

Remark 2.2. Equations (2) and (3) are eikonal equations which, according to the theory of viscosity solutions [11], admit a unique solution in the space of Lipschitz functions $W^{1,\infty}$ on their domain of definition. Since the right-hand side is precisely 1, their solutions are (positive) distance functions to the part of the boundary where a Dirichlet boundary condition is imposed [9], [17]. The streamlines of the vector fields ∇d_{y_i} and $\nabla d_{0,y_i}$ are called rays: they are straight lines, normal to the Dirichlet boundary $\partial\mathcal{B}_{y_i}$ (this can be seen on Fig. 3). Note that rays are well defined if the solutions d_{y_i} and d_{0,y_i} are C^1 smooth. This is the case, at least, in the vicinity of the Dirichlet boundary $\partial\mathcal{B}_{y_i}$ (see Remark 2.5 for more details about this regularity issue).

Let us explain the details of Definition 2.1. First, it clearly depends on the choice of the discrete points $y_i \in \Gamma_D$ and the radius $\epsilon > 0$. The role of the small ball $\mathcal{B}_{y_i}$ around y_i, where a Dirichlet boundary condition is applied, is to send rays from y_i in all directions inside Ω. Indeed, according to Remark 2.2 the streamlines (or rays) of the vector fields ∇d_{y_i} and $\nabla d_{0,y_i}$ are straight lines, normal to the Dirichlet boundary $\partial\mathcal{B}_{y_i}$.

Now let us check that, if $x \in \Gamma_{\text{out}}$ satisfies $d_{y_i}(x) = d_{0,y_i}(x)$, and if ϵ is small enough, then the segment $[xy_i]$ is included in Ω_+ and does not cross the obstacle. Indeed, since Ω is assumed convex, the segment $[xy_i]$ is included in Ω and therefore $d_{0,y_i}(x) = |y_i - x| - \epsilon$, for ϵ small enough, because the straight line is the shortest path. In particular, the rays for d_{0,y_i} are exactly segments $[xy_i]$. If $d_{y_i}(x) = d_{0,y_i}(x)$, it implies that the segment $[xy_i]$ is also included in Ω_+. Conversely, if the segment $[xy_i]$ lies inside Ω_+, then $d_{y_i}(x) = |y_i - x| - \epsilon$, for ϵ small enough. But $[xy_i]$ belongs to Ω too, so $d_{0,y_i}(x) =$

$|y_i - x| - \epsilon$ and thus $d_{y_i}(x) = d_{0,y_i}(x)$. In other words, Definition 2.1, namely checking the equality $d_{y_i}(x) = d_{0,y_i}(x)$, is a discrete version of the original criterion $L_\Sigma(x, y) = |x - y|$ where the discretization parameters are the radius ϵ and the family $y_i \in \Gamma_D$.

2.2. Normal accessibility

In practice, checking Definition 2.1 may be time-consuming since N_y signed distance functions d_{y_i} have to be computed. Therefore, a second definition of accessibility is now introduced, easier and cheaper to use but more restrictive. The main idea is to compute a single distance function d, solution of the new eikonal equation

$$\begin{cases} |\nabla d(x)| &= 1 \quad \text{in } \Omega_+, \\ d &= 0 \quad \text{on } \Gamma_D. \end{cases} \tag{4}$$

Of course, this distance d should be compared with the one without any obstacle, d_0, solution of

$$\begin{cases} |\nabla d_0(x)| &= 1 \quad \text{in } \Omega, \\ d_0 &= 0 \quad \text{on } \Gamma_D. \end{cases} \tag{5}$$

The difference between (4) and (5) is that the first equation takes into account the obstacle Ω_-, contrary to the second one. Of course, for any $x \in \Gamma_{\text{out}}$, one has that $d(x) \geq d_0(x)$. The case of equality gives rise to our second definition.

Definition 2.3 *(Normal accessibility).* A point $x \in \Gamma_{\text{out}}$ is normally accessible if $d(x) = d_0(x)$ where d and d_0 are the solutions of (4) and (5), respectively.

The surface Γ_{out} is normally accessible from Γ_D if any point $x \in \Gamma_{\text{out}}$ is normally accessible from Γ_D.

Let us check that, if $x \in \Gamma_{\text{out}}$ is normally accessible in the sense of Definition 2.3, namely if $d(x) = d_0(x)$, then there exists a point $y \in \Gamma_D$ such that the segment $[xy]$ is contained in Ω_+ and does not cross the obstacle Ω_- (see the left picture in Fig. 2). For any $x \in \Gamma_{\text{out}}$, $d_0(x)$ is its distance to Γ_D. Since Ω is convex, all segments $[xy]$ are included in Ω, for any $y \in \Gamma_D$. Since the straight line is the shortest path, it implies that there exists at least one $y \in \Gamma_D$ such that $d_0(x) = |x - y|$. The equality $d(x) = d_0(x)$ implies that $d(x) = |x - y|$ and therefore the segment $[xy]$ is also the shortest path in Ω_+ and thus does not cross the obstacle Ω_-.

Unfortunately, the converse is not true, i.e., there may exist some choices of Ω, Ω_+ and Γ_D and some points $x \in \Gamma_{\text{out}}$ and $y \in \Gamma_D$ such that the segment $[xy]$ is included in Ω_+ (and is even normal to Γ_D) but $d(x) > d_0(x)$. The reason is that $d_0(x)$ could be strictly smaller than $|x - y|$ as could be the case when Γ_D has two connected components (see Fig. 5 for an example where $d(x) > d_0(x)$ on the lower part of Γ_{out}, although Γ_{out} is obviously normally accessible from Γ_D). A numerical example of this situation and how to correct it is given in Section 6 (see Remark 9.1).

Remark 2.4. Let us explain why Definition 2.3 is called *normal* accessibility. As already said in Remark 2.2, the rays are normal to Γ_D (see Fig. 4), except possibly on the boundary $\partial\Gamma_D$ of Γ_D. Assume that the segment $[xy]$ belongs to Ω_+ and connects the points $x \in \Gamma_{\text{out}}$ and $y \in \Gamma_D$. If $[xy]$ is a ray for (4), and if we ignore the case of rays issued from the boundary of Γ_D, it implies that this ray $[xy]$ is *normal* to Γ_D. In other words, Definition 2.3 can be interpreted as follows: a point $x \in \Gamma_{\text{out}}$ is normally accessible if there exists $y \in \Gamma_D$ such that the segment $[xy]$ is normal to Γ_D and does not intersect the obstacle Ω_-. Of course, this interpretation is slightly incorrect because if $y \in \partial\Gamma_D$ is on the boundary of Γ_D, then the segment $[xy]$ may be not normal.

This definition of normal accessibility is easier to implement numerically because it only requires the computation of two signed distance functions from the starting surface Γ_D. Definition 2.3, being simpler to check and to optimize, is used for most of the following numerical results. Of course, since the segment $[xy]$ must be aligned with the normal to the starting surface Γ_D, Definition 2.3 is more restrictive than the original Definition 2.1, where the segment $[xy]$ can be oriented in any direction with respect to Γ_D.

The difference between these two definitions is illustrated in Fig. 2: the domain Ω is a square with a circular obstacle Ω_- (in red), the starting surface Γ_D is the left side while the target surface Γ_{out} is the right side of the square. The picture on the left is concerned with the normal accessibility of Definition 2.3: in particular, the point x_1 is not normally accessible from Γ_D since the segment $[x_1 y_1]$ normal to Γ_D cut Ω_-. On the other hand, the point x_2 is normally accessible from Γ_D, and more precisely from y_2. The picture on the right is concerned with the multi-directional accessibility of Definition 2.1: of course, the point x_2 is still multi-directionally accessible from y_2, but the point x_1 is now multi-directionally accessible from y_2 (but not from y_1). The segment $[x_1 y_2]$ is not normal to Γ_D but it does not matter in Definition 2.1.

Remark 2.5. The same existence result holds for (4) and (5) as for previous eikonal equations discussed in Remark 2.2. Rays are defined in a similar manner. For simplicity, let us focus on the solution d_0 of (5). The viscosity solution d_0 is defined in the space of Lipschitz functions $W^{1,\infty}(\Omega)$. Thus, d_0 is continuous in Ω but its gradient is not, in full generality. The set of

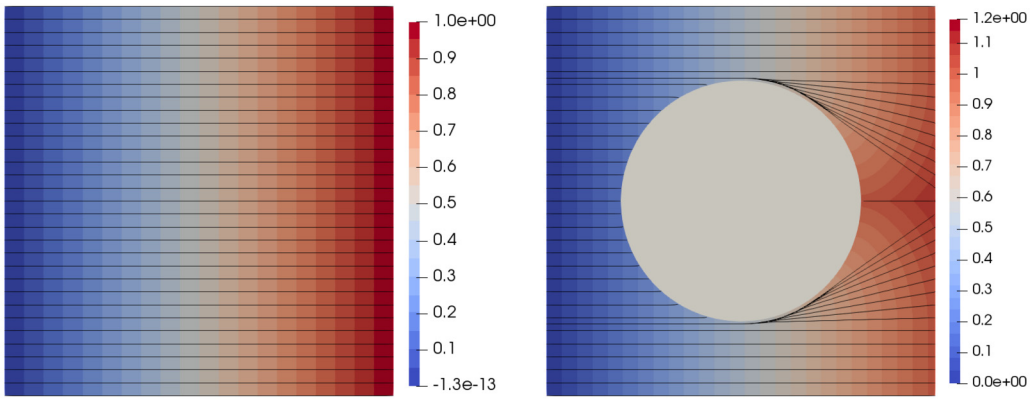

Fig. 4. Streamlines or rays of d_0 (left, without obstacle) and d (right, with obstacle) issued from the left side Γ_D.

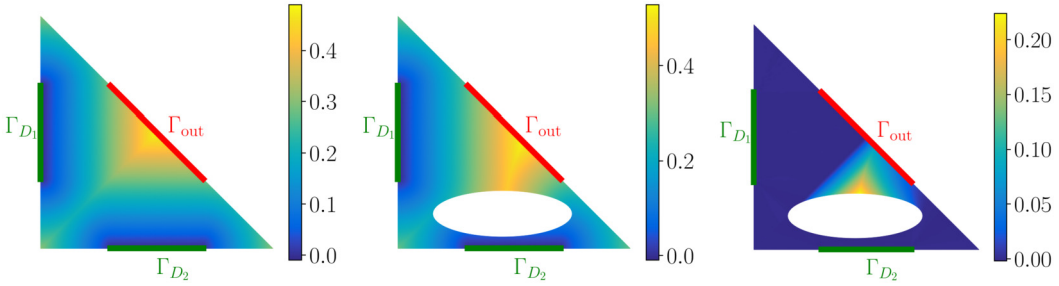

Fig. 5. An example of a triangular domain with a white ellipsoidal obstacle Ω_-, where Definition 2.3 fails to detect a segment connecting Γ_D (in green, with two connected components Γ_{D_1} and Γ_{D_2}) to Γ_{out} (in red). Distance d_0 (left), distance d (middle), difference $d - d_0$ (right).

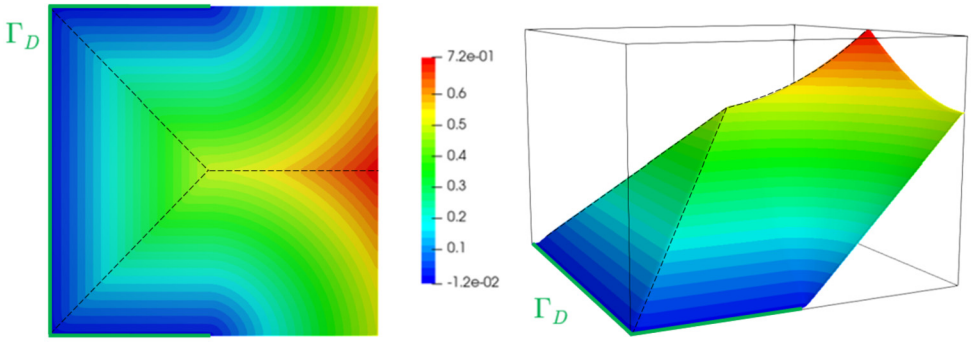

Fig. 6. Skeleton (black line) of the distance function for Γ_D, being the left part of the boundary: 2-d view (left) and 3-d view (right) of the distance function.

points in Ω where d_0 is not differentiable is called the skeleton: equivalently, it is the set of ridges of d_0 and it is a set of zero-measure in Ω (see [9] and [17], or [7] in the context of topology optimization). An example of a skeleton is plotted on Fig. 6 for a square domain $\Omega = (0, 1)^2$ (with a cartesian mesh of size 0.005) and a boundary $\Gamma_D = \partial\Omega \cap \{x_1 < 0.5\}$ which is the left half of $\partial\Omega$.

Remark 2.6. We close this section by emphasizing that the convexity assumption on Ω is crucial to interpret Definitions 2.1 and 2.3. It is because of convexity that equality between two distances, with and without the obstacle, implies that a segment connect points $x \in \Gamma_{\text{out}}$ and $y \in \Gamma_D$.

2.3. Eikonal equation with a penalized obstacle

A key ingredient in the numerical verification of the accessibility definitions of the previous subsections is the computation of a signed distance function inside Ω_+. Although this computation does not pose any fundamental difficulty, on the contrary the derivation of this signed distance function with respect to the position of the interface Σ (the boundary of the obstacle Ω_-) is a difficult problem for which we do not have a solution. Therefore, we circumvent this hurdle by replacing

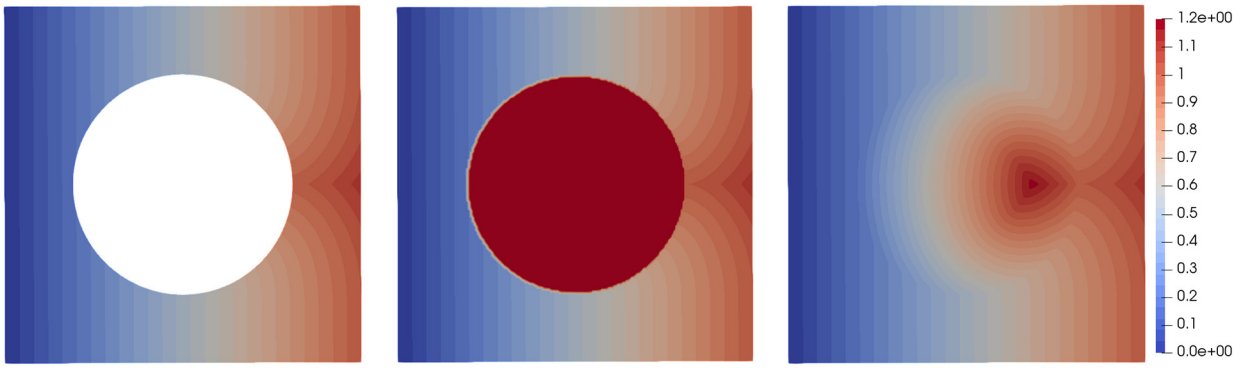

Fig. 7. Solution of (7) computed in Ω_+ only (left), in the complete domain Ω with $V_- = 0.001$ (middle) and with $V_- = 0.5$ (right). In all cases $V_+ = 1$.

the obstacle Ω_- with a different medium where the metric induces larger distances. More precisely, we introduce a normal speed function $V(x) : \Omega \to \mathbb{R}^+$, defined by

$$V(x) = \begin{cases} V_+ & \text{in } \Omega_+, \\ V_- & \text{in } \Omega_-, \end{cases} \tag{6}$$

with $V_+ > V_- > 0$ (in the sequel $V_+ = 1$), meaning that the speed is smaller in the obstacle, yielding larger values of the distance when crossing the obstacle. In other words, instead of having a zero speed in Ω_-, the obstacle is filled with an "ersatz" material which has a small, but yet non-vanishing, velocity. It can be interpreted as a penalization approach for taking into account the obstacle. Therefore, in the sequel equation (4) is replaced by its penalized version

$$\begin{cases} V(x)|\nabla d(x)| &= 1 \quad \text{in } \Omega, \\ d &= 0 \quad \text{on } \Gamma_D. \end{cases} \tag{7}$$

Remark 2.7. If the interface Σ is C^1 smooth, then the same existence result holds for (7) as for previous eikonal equations discussed in Remark 2.2. Rays are defined in a similar manner. The same regularity results, as presented in Remark 2.5, hold true. In particular viscosity solutions for these eikonal equations are defined in $W^{1,\infty}(\Omega)$. Thus, the solution d of (7) is continuous in Ω but its gradient is not, in full generality. As before, the set of points in Ω where d is not differentiable is called the skeleton and it is a set of zero-measure in Ω. Of course, the interface Σ belongs to the skeleton because, the velocity being discontinuous on Σ, necessarily ∇d is discontinuous on Σ too. In the following we always assume that all distance functions d and d_{y_i} are smooth, except on their skeletons.

Note that for any value of V_-, strictly smaller than V_+, the two accessibility criteria of Definitions 2.1 and 2.3 give the same notion of accessibility if the distance d is computed as the solution of (7) instead of (4). To assess the approximation of an obstacle with a small velocity, we consider the geometry and boundary conditions of Fig. 2 (a square domain $\Omega = (0, 1)^2$ with a circular obstacle of radius $r = 0.31$ and a cartesian mesh of size $h = 0.005$). On Fig. 7 we plot the signed distance function, solution of (7), for two different values of the velocity $V_- = 0.5$ and $V_- = 0.001$, as well as for the perforated domain Ω_+ alone. Clearly, the level-sets of d are distorted by the obstacle. The presence of the obstacle or the small speed inside Ω_- induces an increase of the values of the signed distance inside and behind the obstacle. This effect is visible even for not so small values of V_-. The middle solution (with $V_- = 0.001$) is very similar to the solution in the perforated domain (left), confirming that the approximation of a real obstacle by a medium with a smaller speed is reasonable. Actually, it is expected that for a given smooth obstacle, there is a threshold value of V_- such that, below this value, all solutions of (7) give the same distances in Ω_+.

The same penalization approach is applied to the other eikonal equations involving the obstacle Ω^-. For example, equation (2) is replaced in the sequel by its penalized version

$$\begin{cases} V(x)|\nabla d_{y_i}(x)| &= 1 \quad \text{in } \Omega \setminus \mathcal{B}_{y_i}, \\ d_{y_i} &= 0 \quad \text{on } \partial\mathcal{B}_{y_i}. \end{cases} \tag{8}$$

3. Accessibility criteria

Given the two definitions of accessibility introduced in Section 2, we propose two criteria, one for each definition, in order to quantify their fulfillment. We start with the easiest case of normal accessibility.

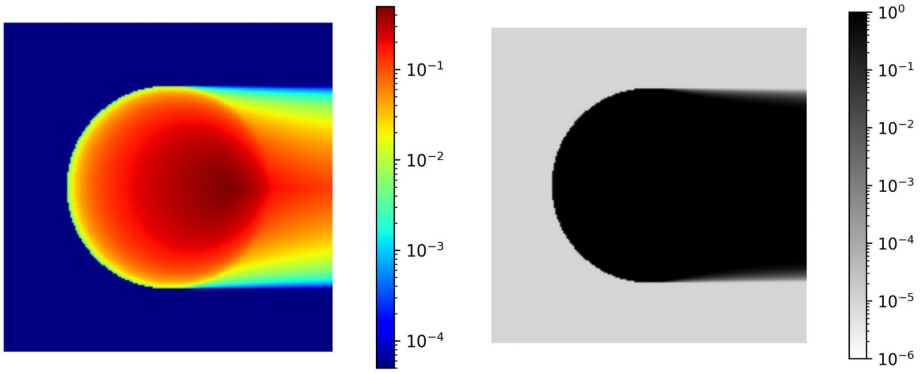

Fig. 8. Plots of the fields $d - d_0$ (left) and $h_\varepsilon(d - d_0)$ (right), showing the non-accessible points on Γ_{out}.

3.1. Normal accessibility criterion

In the context of Definition 2.3, a target surface Γ_{out} is normally accessible if, for any $x \in \Gamma_{\text{out}}$, the equality $d(x) = d_0(x)$ holds true, where d_0 is the reference distance function in the domain Ω without obstacle (solution of (5)) and d is the distance function, taking into account the obstacle, solution of (7). The simplest idea to evaluate the normal accessibility is to use a least-square criterion:

$$J_1(\Sigma) = \int_{\Gamma_{\text{out}}} |d - d_0|^2 ds, \tag{9}$$

where clearly $J_1(\Sigma) = 0$ if and only if Γ_{out} is normally accessible. For the example of Figs. 2 and 7 (with a cartesian mesh of size $h = 0.005$) the (non-negative) field $d - d_0$ is shown in Fig. 8 (left) for the speed $V_- = 0.5$. One can see that the values of $d - d_0$ are varying a lot: they are larger in the middle of the shadow of the obstacle on the right side Γ_{out} than on the borders of this shadow region. However, the accessibility criteria is binary and it is violated as soon as $d(x) - d_0(x) > 0$, whatever the value of this positive difference.

Therefore, we suggest another criterion which relies on a Heaviside function applied to $(d - d_0)$ before integrating it on Γ_{out}. For optimization purposes (related to differentiability), this Heaviside function is regularized using a small parameter $\varepsilon > 0$ of the order of the mesh size (ε is different and should not be confused with the other parameter ϵ which is the radius of the small balls $\mathcal{B}_{y_i}$ in Definition 2.1 of multi-directional accessibility). The regularized Heaviside function is denoted by h_ε, defined as:

$$h_\varepsilon(z) = \begin{cases} 0 & \text{if } z < 0, \\ \dfrac{1}{2} + \dfrac{1}{2}\sin\left(\dfrac{\pi z}{\varepsilon} - \dfrac{\pi}{2}\right) & \text{if } 0 \le z \le \varepsilon, \\ 1 & \text{if } z > \varepsilon. \end{cases} \tag{10}$$

For the example of Figs. 2 and 7 the function $h_\varepsilon(d - d_0)$, with $\varepsilon = 2h$ (twice the mesh size), is shown in Fig. 8 (right) where it can be checked that this function is much more uniform, except in a thin region of size ε close to the borders of the shadow region. The new criterion is then defined by

$$J_{1,\varepsilon}(\Sigma) = \int_{\Gamma_{\text{out}}} h_\varepsilon\,(d - d_0)\, ds. \tag{11}$$

Both criteria (9) and (11) can be rewritten as

$$J(\Sigma) = \int_{\Gamma_{\text{out}}} k(d)\, ds, \tag{12}$$

where k is a smooth function from $\mathbb{R}^+$ to $\mathbb{R}^+$. For the sake of notational simplicity the reference distance d_0 is not explicitly written in the functional (12), although all our examples depend on the difference $d - d_0$. This is not an issue since the reference distance d_0 does not depend on Σ.

3.2. Multi-directional accessibility criterion

We now give a criterion for the multi-directional accessibility of Definition 2.1. Recall that, upon discretization of the starting surface Γ_D by points y_i, $1 \le i \le N_y$, the target surface Γ_{out} is multi-directionally accessible from Γ_D if, for any

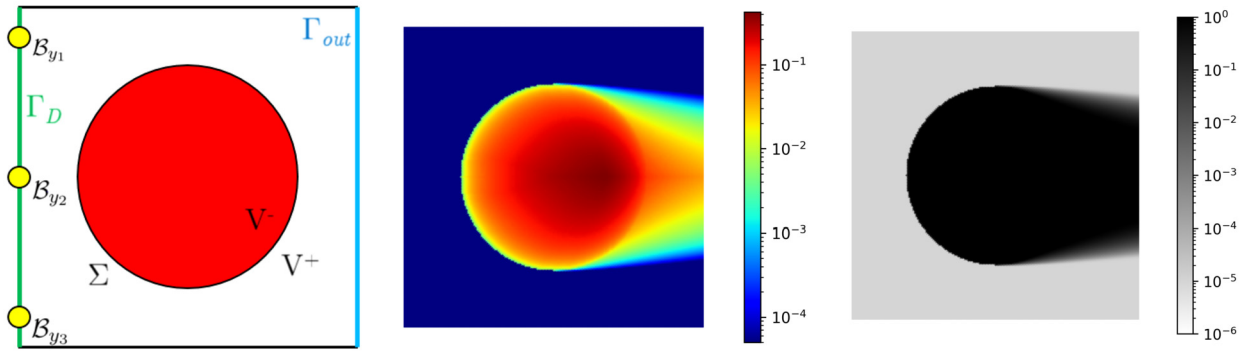

Fig. 9. Accessibility of Γ_{out}, measured from three points on Γ_D, with a red obstacle (left): fields $\min_{i=1,2,3}(d_{y_i} - d_{0,y_i})$ (middle) and $h_\varepsilon\left(\min_{i=1,2,3}(d_{y_i} - d_{0,y_i})\right)$ (right).

$x \in \Gamma_{\text{out}}$, there exists at least one point y_i such that $d_{y_i}(x) = d_{0,y_i}(x)$, where d_{y_i} is the solution of (8) and d_{0,y_i} is the solution of (3). A simple criterion to evaluate this definition is again a least-square function

$$J_2(\Sigma) = \int_{\Gamma_{\text{out}}} \left| \min_{i=1,\dots,N_y} (d_{y_i} - d_{0,y_i}) \right|^2 ds, \tag{13}$$

where the minimum operator in (13) is a consequence of the fact that the existence of just one point y_i, such that $d_{y_i}(x) = d_{0,y_i}(x)$, is enough for multi-directional accessibility. As before, since $d_{y_i}(x) \geq d_{0,y_i}(x)$ for any $x \in \Gamma_{\text{out}}$, one can replace the square by the regularized Heaviside function h_ε for the integrand of (13) in order to assign almost the same value to all inaccessible points. The new criterion is then defined by

$$J_{2,\varepsilon}(\Sigma) = \int_{\Gamma_{\text{out}}} h_\varepsilon\left(\min_{i=1,\dots,N_y} (d_{y_i} - d_{0,y_i}) \right) ds. \tag{14}$$

To understand the difference between these two criteria, we study the example of Fig. 9 (left) where the accessibility of the right side Γ_{out} of the square $\Omega = (0,1)^2$ is evaluated with three points $(y_1, y_2, y_3) \in \Gamma_D$ uniformly distributed on the left side. Three balls $(\mathcal{B}_{y_1}, \mathcal{B}_{y_2}, \mathcal{B}_{y_3})$ of radius 0.03 (for a mesh size of 0.005) are shown in yellow. Furthermore, the circular obstacle of radius $r = 0.31$ (in red) features a speed $V_- = 0.5$. The fields $\min_{i=1,2,3}(d_{y_i} - d_{0,y_i})$, plotted in Fig. 9 (middle), and $h_\varepsilon\left(\min_{i=1,2,3}(d_{y_i} - d_{0,y_i})\right)$, plotted in Fig. 9 (right) for $\varepsilon = 2h$, highlight the non-accessible zone from the points $(y_1, y_2, y_3) \in \Gamma_D$.

The minimum operator is not differentiable but, in practice, we ignore the non-differentiability of the minimum. In other words, for a function $f = \min(f_1, f_2)$ the following approximation is made: $f' = f_1'$ if $f_1 < f_2$ and $f' = f_2'$ if $f_2 < f_1$ and we ignore the case when $f_1 = f_2$.

4. Shape derivative with respect to the obstacle

4.1. Case of normal accessibility

We place ourselves in the setting of Definition 2.3 of normal accessibility. Consider a functional of the interface Σ (the boundary of the obstacle Ω_-) which is defined by

$$J(\Sigma) = \int_{\Omega} j(d)dx + \int_{\Gamma_{\text{out}}} k(d)ds, \tag{15}$$

where j, k are smooth real functions and d is the signed distance function, solution of (7), which thus depends on Σ. Note that for most of our applications we have $j = 0$ or j supported in a smaller subset of Ω. The goal of this section is to compute the shape derivative of (15). Our analysis will be mostly formal since a rigorous proof of differentiability is out of our reach for technical reasons.

In the framework of the Hadamard method of shape sensitivity (see [5], [25]), we introduce vector fields $\theta \in W^{1,\infty}(\Omega; \mathbb{R}^d)$ which vanish on $\partial\Omega$. We consider variations of the interface of the type $\Sigma_\theta = (Id + \theta)\Sigma$, which induces the following variation of the speed

$$V_\theta(x) = \begin{cases} V_+ & \text{in } (Id+\theta)\Omega_+, \\ V_- & \text{in } (Id+\theta)\Omega_-. \end{cases} \tag{16}$$

The shape derivative of $J(\Sigma)$ is then defined as the derivative of $\theta \mapsto J(\Sigma_\theta)$ at 0. As a first step, since $J(\Sigma)$ depends on the signed distance function d, one must differentiate the solution d of (7). Differentiating distance function with respect to their domain of definition Ω is a classical matter (see e.g. [18], [3]). However, differentiating with respect to the interface Σ, where the velocity $V(x)$ is discontinuous, is new, to the best of our knowledge.

Lemma 4.1. *Assume the interface Σ is smooth. Let d be the signed distance function, solution of (7). Fix a point $x \in \Omega$ which does not belong to the skeleton of d (see Remark 2.5 for its definition). Then $\theta \mapsto d_{(Id+\theta)\Omega}(x)$ is Gâteaux-differentiable at $\theta = 0$, as an application from $W^{1,\infty}(D, \mathbb{R}^d)$ into $\mathbb{R}$, and its directional derivative, denoted by $d'(x) = \langle d'(\Sigma), \theta \rangle$, is the solution of*

$$\left\{\begin{array}{rcl} V_+ \nabla d_+ \cdot \nabla d'_+ & = & 0 \quad \text{in } \Omega_+, \\ V_- \nabla d_- \cdot \nabla d'_- & = & 0 \quad \text{in } \Omega_-, \\ d'_+ & = & 0 \quad \text{on } \Gamma_D, \\ d'_- - d'_+ + (n \cdot \nabla d_- - n \cdot \nabla d_+)\theta \cdot n & = & 0 \quad \text{on } \Sigma, \end{array}\right. \tag{17}$$

where the indices $+$ or $-$ indicate the restriction of a function to the subdomains Ω_+ or Ω_-.

In truth, our proof of Lemma 4.1 is merely formal, in particular because the existence and uniqueness of the solution d' of (17) is not completely understood (by us) as explained in the following remark.

Remark 4.2. Obviously (17) is a linear transport equation for d' with a unit velocity field $V \nabla d$ and a Dirichlet boundary condition on Γ_D and a transmission condition on Σ. There are two difficulties for the well-posedness of (17). First, the solution d' is discontinuous through Σ, in full generality. Secondly, and this is the most serious difficulty, the velocity field is not Lipschitz or even differentiable, worse it is discontinuous on Σ and on the skeleton of d. Therefore, there is no classical existence (not to mention uniqueness) theory we can apply. The first difficulty is not so much a problem since the transmission condition on Σ could be interpreted as an ingoing Dirichlet boundary condition to compute d'_- in terms d'_+, or vice-versa, depending on the sign of the normal component of the velocity $V \nabla d$. The second difficulty is more severe. Again, the velocity discontinuity through Σ is not a real issue because of the transmission condition on Σ. However, the discontinuity through the skeleton is problematic. There are some results about transport equations with discontinuous coefficients [13,26], but we do not know how they could be applied in the present case. Nevertheless, in the sequel we shall assume that (17) admits a unique solution $d' \in L^\infty(\Omega)$. Note that, at least, the vector field is ingoing on Γ_D, meaning that $V \nabla d \cdot n < 0$ on Γ_D, and outgoing on $\Gamma_c \cup \Gamma_{\text{out}}$, meaning that $V \nabla d \cdot n \geq 0$ on $\Gamma_c \cup \Gamma_{\text{out}}$.

Proof. We content ourselves in giving a formal proof. Rewriting (7) in each subdomain and squaring it, yields

$$\left\{\begin{array}{rcll} V_+^2 |\nabla d_+|^2 & = & 1 & \text{in } \Omega_+, \\ V_-^2 |\nabla d_-|^2 & = & 1 & \text{in } \Omega_-, \\ d_+ & = & 0 & \text{on } \Gamma_D, \\ d_+ & = & d_- & \text{on } \Sigma. \end{array}\right. \tag{18}$$

Assuming that d_+ and d_- are shape differentiable with respect to Σ, we seek the equation satisfied by the directional derivative $d' = \langle d'(\Sigma), \theta \rangle$. Differentiating (18) with respect to Σ in the direction θ [18,3] leads to

$$\left\{\begin{array}{rcll} V_+^2 \nabla d_+ \cdot \nabla d'_+ & = & 0 & \text{in } \Omega_+, \\ V_-^2 \nabla d_- \cdot \nabla d'_- & = & 0 & \text{in } \Omega_-, \\ d'_+ & = & 0 & \text{on } \Gamma_D. \end{array}\right. \tag{19}$$

Since the right-hand side of (19) is zero, it is possible to divide the two first lines by $V_\pm$ in order to deduce the same two first lines of (17). To recover a transmission condition for d' on the interface Σ, we rewrite the continuity, $d_- = d_+$ on Σ, under a weak form: for any smooth test function φ, we have

$$\int_\Sigma (d_- - d_+)\varphi \, ds = 0.$$

Then, differentiating with respect to Σ in the direction θ gives

$$\int_\Sigma (d'_- - d'_+)\varphi \, ds + \int_\Sigma \left(\frac{\partial}{\partial n} + H\right)\big((d_- - d_+)\varphi\big)\theta \cdot n \, ds = 0,$$

where n is the unit normal vector to Σ and $H = \operatorname{div} n$ is the mean curvature. Since $d_+ = d_-$ on Σ, we get

$$\int_\Sigma \varphi \left((d'_- - d'_+) + \frac{\partial (d_- - d_+)}{\partial n}\theta \cdot n\right) ds = 0,$$

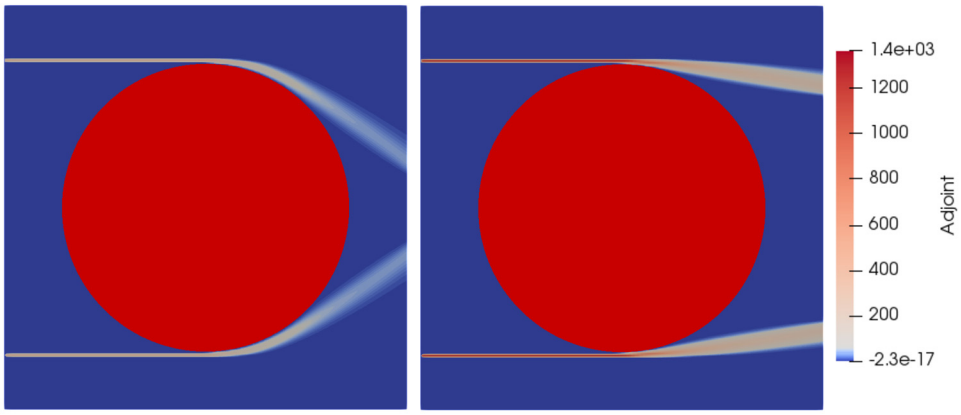

Fig. 10. Adjoint state p, solution of (20) for a circular obstacle and $J_1(\Sigma)$ (left) or $J_{1,\varepsilon}(\Sigma)$ (right).

which yields the desired system (17). □

To compute the shape derivative and eliminate the derivative d', an adjoint equation for (7) and (15) is required. As usual, it is a linear equation whose solution, denoted by p, turns out to be discontinuous at the interface Σ. Therefore, we introduce p_+ as the restriction of p in Ω_+ and p_- as the restriction of p in Ω_- (a similar notation d_+, d_- is used for the distance function d). The adjoint p is a solution of

$$\left\{\begin{array}{rcll} -\mathrm{div}\,(V_+ p_+ \nabla d_+) & = & j'(d_+) & \text{in } \Omega_+, \\ -\mathrm{div}\,(V_- p_- \nabla d_-) & = & j'(d_-) & \text{in } \Omega_-, \\ p_+ & = & k'(d)/(V\nabla d\cdot n) & \text{on } \Gamma_{\mathrm{out}}, \\ p_+ & = & 0 & \text{on } \Gamma_c, \\ V_+ p_+ \nabla d_+ \cdot n & = & V_- p_- \nabla d_- \cdot n & \text{on } \Sigma. \end{array}\right. \tag{20}$$

Remark 4.3. The adjoint equation (20) is a linear transport equation for p under conservative form. Note the change of sign of the vectorial velocity which is $-V\nabla d$. In other words, the adjoint equation is "backward" compared to the original transport equation (7). In particular, (20) features Dirichlet boundary conditions on the inflow boundaries $\Gamma_{\mathrm{out}} \cup \Gamma_c$ and no boundary condition on the outflow boundary Γ_D. Indeed, one can check that the solution d of (7) satisfies $-V\nabla d\cdot n \le 0$ on $\Gamma_{\mathrm{out}} \cup \Gamma_c$, as well as $-V\nabla d\cdot n > 0$ on Γ_D. The last line of (20) is a transmission condition on Σ which ensures that the vector field $-Vp\nabla d$ has a continuous normal component through Σ (in particular, it implies that the two first lines of (20) are equivalent to $-\mathrm{div}\,(Vp\nabla d) = j'(d)$ in Ω). As already said in Remark 4.2 the velocity field $-V\nabla d$ is not continuous on the skeleton of d which is a difficulty for proving that the adjoint equation (20) admits a unique solution p. Nevertheless, we shall explain in Subsection 7.1 how its solution can be numerically computed. For the geometrical setting of Fig. 2 (a circular obstacle) and for normal accessibility, the adjoint p, solution of (20) for the objective function $J_{1,\varepsilon}(\Sigma)$, is shown in Fig. 10. There, one can see a focusing effect for the streamlines of the vector field $-V\nabla d$, indicating that the solution p is not continuous and maybe is not a function but rather a measure (see [10], [13], [26]).

Proposition 4.4. *The functional $J(\Sigma)$, defined by (15), is shape differentiable and its derivative is written, for any $\theta \in W^{1,\infty}(\Omega;\mathbb{R}^d)$,*

$$\langle J'(\Sigma),\theta\rangle = \int_\Sigma V_+\nabla d_+\cdot n_+ p_+ n\cdot(\nabla d_+ - \nabla d_-)\,\theta\cdot n\,ds \tag{21}$$

with d_+, d_-, the solution of (7), and p_+ the adjoint state, solution of (20). Moreover, n_+, respectively n_-, are the outer unit normal vectors to Ω_+, respectively Ω_-, and we choose $n = n_-$ as the normal vector to Σ.

Proof. Once we have assumed Lemma 4.1 and that both linear transport equations (17) and (20) are well posed, the rest of the proof is rigorous. By the chain rule lemma, the shape derivative of (15) is

$$\langle J'(\Sigma),\theta\rangle = \int_\Omega j'(d)\,d'\,dx + \int_{\Gamma_{\mathrm{out}}} k'(d)\,d'\,ds. \tag{22}$$

To eliminate d' we use the adjoint equation (20). Multiplying (20) by d' and integrating by parts separately in Ω_+ and Ω_-, we get

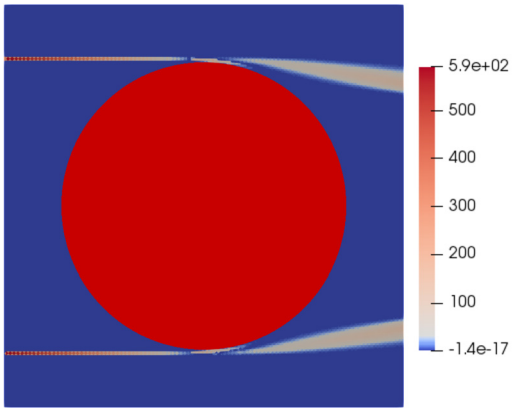

Fig. 11. Integrand of the shape derivative (21) for $J_{1,\varepsilon}(\Sigma)$ and a circular obstacle.

$$\int_{\Omega_+} V_+\nabla d_+\cdot\nabla d'_+ p_+\,dx - \int_{\partial\Omega_+} V_+\nabla d_+\cdot n_+ p_+ d'_+\,ds$$
$$+\int_{\Omega_-} V_-\nabla d_-\cdot\nabla d'_- p_-\,dx - \int_{\partial\Omega_-} V_-\nabla d_-\cdot n_- p_- d'_-\,ds \;=\int_{\Omega} j'(d)d'\,dx.$$

The two integrals on Ω_+ and Ω_- cancel because of equation (17). Since $\partial\Omega_+\cup\partial\Omega_-=\partial\Omega\cup\Sigma$, we treat separately the integrals on $\partial\Omega$ and on Σ. The integral on $\partial\Omega$ is reduced to an integral on $\Gamma_{\rm out}$ because of the Dirichlet boundary conditions in (20) and (17). To simplify the integral on Σ we use the transmission condition for p in (20). It yields

$$-\int_{\Sigma}(d'_+-d'_-)V_+\nabla d_+\cdot n_+ p_+\,ds=\int_{\Omega} j'(d)d'\,dx+\int_{\Gamma_{\rm out}} k'(d)d'\,ds.$$

Then, using the transmission condition for d' on Σ in (17), we get

$$-\int_{\Sigma} n\cdot(\nabla d_- -\nabla d_+)\theta\cdot nV_+\nabla d_+\cdot n_+ p_+\,ds=\int_{\Omega} j'(d)d'\,dx+\int_{\Gamma_{\rm out}} k'(d)d'\,ds,$$

which, combined to (22), leads to the desired formula for the shape derivative. □

Remark 4.5. In line with Remark 4.3 where we questioned the smoothness of the adjoint p, one can wonder about the regularity of the integrand in formula (21) for the shape derivative. Clearly, if p is not smooth (for example, is a measure), then this integrand cannot be smoother. But there is more to say on the structure of this shape derivative. To fix ideas, let us consider again the geometric setting of Fig. 2 (a circular obstacle) and the objective function $J_{1,\varepsilon}(\Sigma)$, which measures accessibility of the right side from the left side. For this geometry the integrand of the shape derivative is plotted on Fig. 11 where one can see that it is concentrated near the north and south poles of the circular obstacle. Indeed, changing the lateral shape of the obstacle will not produce any change in the objective function and it is intuitively clear that only boundary variations on the upper and lower part of the obstacle boundary can induce a modification of $J_{1,\varepsilon}(\Sigma)$. Since the shape derivative can be a measure, the rigorous justification of Proposition 4.4 is therefore not obvious.

We now recall a result known as Snell's law which allows us to give a more convient formula for the shape derivative which is used in numerical practice.

Lemma 4.6. *Assume that the interface Σ is smooth. Let d be the unique solution in $W^{1,\infty}(\Omega)$ of (7) and $n=n_-$ be the outward unit normal to Ω_-. Denote by α_+ the angle made by $V_+\nabla d_+$ with n on Σ and α_- defined in the same way for $V_-\nabla d_-$. Then*

$$\frac{\sin\alpha_+}{\sin\alpha_-}=\frac{V_+}{V_-}. \tag{23}$$

Proof. Since the traces satisfy $d_-=d_+$ on Σ, the tangential components of ∇d_+ and ∇d_- are also equal on Σ. Since $V\nabla d$ is a unit vector, the angles α_+ and α_- are defined on Σ by

$$\cos\alpha_+ = -V_+\nabla d_+ \cdot n \quad \text{and} \quad \cos\alpha_- = -V_-\nabla d_- \cdot n$$

The above sign is chosen such that, if the rays going from Ω_+ into Ω_-, then the angles α_+ and α_- belong to the range $(0, \pi/2)$. The tangential components of ∇d_+ and ∇d_- being equal, it implies that $\frac{\sin\alpha_+}{V_+} = \frac{\sin\alpha_-}{V_-}$, which is precisely Snell's law. □

Corollary 4.7. *The shape derivative of Proposition 4.4 is equivalently defined by*

$$\langle J'(\Sigma), \theta\rangle = -\int_\Sigma \left(\frac{1}{V_+}\cos\alpha_+ - \frac{1}{V_-}\cos\alpha_-\right) p_+ \cos\alpha_+ \theta\cdot n\, ds, \tag{24}$$

where α_+ is the angle made by n with $V_+\nabla d_+$ on Σ, and

$$\cos\alpha_- = \sqrt{1 - \sin^2\alpha_+ \frac{V_-^2}{V_+^2}} = \frac{\sqrt{V_+^2 - V_-^2 + \cos\alpha_+^2 V_-^2}}{V_+}.$$

Proof. Formula (24) is an immediate consequence of the definitions of the angles in Lemma 4.6. By Snell's law (23) one deduce the formula for $\cos\alpha_-$.

The main interest of (24) is that it depends only on d_+ and not anymore on d_-. Thus, from a numerical point of view it is easier to evaluate. □

4.2. Case of multi-directional accessibility

We now consider the setting of Definition 2.1 of multi-directional accessibility, which is evaluated by computing the collections of signed distance function d_{y_i}, solution of (8). Consider a functional of the interface Σ, defined by

$$J(\Sigma) = \int_\Omega j(d_{y_1}, ..., d_{y_{N_y}})dx + \int_{\Gamma_{\text{out}}} k(d_{y_1}, ..., d_{y_{N_y}})ds, \tag{25}$$

where $j, k : \mathbb{R}^{N_y} \to \mathbb{R}$ are smooth functions and $(d_{y_1}, ..., d_{y_{N_y}})$ is the family of solutions of (8), which depend on Σ.

In this case, the family of adjoint equations, indexed by $1 \le i \le N_y$, is written as

$$\begin{cases} -\text{div}\,(V p_{y_i}\nabla d_{y_i}) &= \partial_i j & \text{in } \Omega, \\ p_{y_i} &= \frac{\partial_i k}{V\nabla d_{y_i}\cdot n} & \text{on } \Gamma_{\text{out}}, \\ p_{y_i} &= 0 & \text{on } \Gamma_c, \\ V_+ p_{y_i+}\nabla d_{y_i+}\cdot n &= V_- p_{y_i-}\nabla d_{y_i-}\cdot n & \text{on } \Sigma, \end{cases} \tag{26}$$

where $\partial_i j = \frac{\partial j}{\partial d_{y_i}}(d_{y_1}, ..., d_{y_{N_y}})$ and similarly for $\partial_i k$. Equation (26) is very similar to the previous adjoint equation (20). It is a transport equation under conservative form which admits a unique solution $p_{y_i} \in L^\infty(\Omega)$.

Proposition 4.8. *The function $J(\Sigma)$, defined by (25), is shape differentiable and, for any $\theta \in W^{1,\infty}(\Omega; \mathbb{R}^d)$, its derivative is given by*

$$\langle J'(\Sigma), \theta\rangle = \int_\Sigma \theta\cdot n V_+ \left(\sum_{i=1}^{N_y} \nabla d_{y_i+}\cdot n_+ p_{y_i+} n\cdot(\nabla d_{y_i+} - \nabla d_{y_i-})\right) ds, \tag{27}$$

with d_{y_i+}, respectively d_{y_i-}, the solution of (8) in Ω_+, respectively in Ω_- and p_{y_i+} the adjoint state in Ω_+, solution of (26).

The proof of Proposition 4.8 is completely similar to that of Proposition 4.4, so we omit it.

5. Shape derivative with respect to the target surface

In this section the target surface Γ_{out} is the optimization variable and the goal is to compute a shape derivative with respect to Γ_{out}. We consider two different scenarios: first, the obstacle Ω_- is fixed, second, the boundary of the obstacle is equal to the target surface. Only the normal accessibility is detailed: our results can easily be extended to the multi-directional accessibility as explained in Remark 5.5.

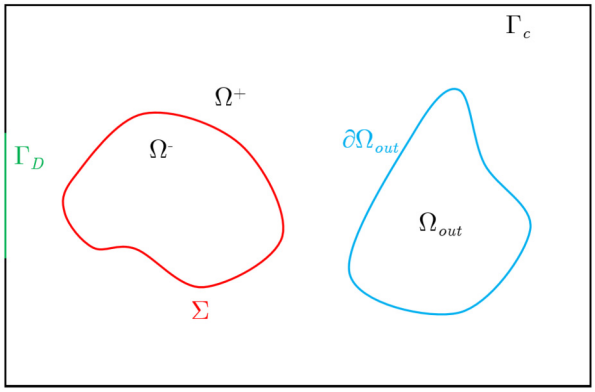

Fig. 12. Domain Ω with a fixed obstacle Ω_- and a varying subdomain $\Omega_{\rm out} \subset \Omega_+$.

5.1. Fixed obstacle

In this subsection the shape of the obstacle is assumed to be fixed and the target surface $\Gamma_{\rm out}$ is the only optimization variable. To comply with the numerical applications which will be addressed later in Section 8, we slightly change the geometrical setting from Fig. 1 to Fig. 12. In this new setting the target surface $\Gamma_{\rm out}$ is the boundary of a new subdomain $\Omega_{\rm out} \subset \Omega_+$ and the boundary of the full domain Ω reduces to $\partial\Omega = \Gamma_D \cup \Gamma_c$. More precisely, Ω is still divided in two disjoint subsets, $\Omega = \Omega_+ \cup \Sigma \cup \Omega_-$, with $\Omega_{\rm out} \subset \Omega_+$ and $\Gamma_{\rm out} = \partial\Omega_{\rm out}$.

The previous objective function (15) is changed to a new one

$$J(\Omega_{\rm out}) = \int_{\Omega_{\rm out}} j(d)\,dx + \int_{\partial\Omega_{\rm out}} k(d)\,ds, \tag{28}$$

where j, k are smooth real functions and d is the distance function, solution of (7). It turns out that equation (7) is independent of $\Omega_{\rm out}$, as well as all other eikonal equations studied here. Therefore the distance d does not depend on $\Omega_{\rm out}$ and the computation of the shape derivative of (28) is much easier. Note in passing that the objective function J is written as a function of $\Omega_{\rm out}$ but it could equivalently be considered as a function of $\Gamma_{\rm out} = \partial\Omega_{\rm out}$.

Proposition 5.1. *The objective function (28) is shape differentiable and its derivative, for any $\theta \in W^{1,\infty}(\Omega;\mathbb{R}^d)$, is given by*

$$\langle J'(\Omega_{out}), \theta\rangle = \int_{\partial\Omega_{out}} j(d)\,\theta\cdot n\,ds + \int_{\partial\Omega_{out}} \left(\frac{\partial k(d)}{\partial n} + Hk(d)\right)\theta\cdot n\,ds, \tag{29}$$

where n is the outer unit normal vector of $\partial\Omega_{out}$ and $H = \operatorname{div} n$ is the mean curvature.

Proof. It is a direct application of standard results in shape optimization (see Theorems 4.2 and 4.3 in [5]) since the distance function d does not depend on $\Omega_{\rm out}$. □

Remark 5.2. If both the obstacle Ω_- (characterized by its boundary Σ) and the target $\Omega_{\rm out}$ are optimized independently and if they do not intersect, $\Omega_- \cap \Omega_{\rm out} = \emptyset$, then the partial derivatives of an objective function $J(\Sigma, \Omega_{\rm out})$ are given by Proposition 4.4 for the one with respect to Σ and by Proposition 5.1 for the other one with respect to $\Omega_{\rm out}$. The case when the obstacle and target are complementary, $\Omega = \Omega_- \cup \Omega_{\rm out}$, is discussed in the next subsection.

5.2. Complementary obstacle and target

In this subsection the obstacle and the target volume are assumed to be complementary, $\Omega_{\rm out} = \Omega_+ = \Omega \setminus \Omega_-$. In other words, accessibility is evaluated on the boundary $\Gamma_{\rm out} = \Sigma$ of the obstacle (a situation which is precisely the relevant one for mechanical applications in Section 9). The previous objective function (28) is changed to a new one

$$J(\Sigma) = \int_{\Omega_{\rm out}} j(d)\,dx, \tag{30}$$

where j is a smooth function and d is the distance function, solution of (7). The novelty in (30) is that, the integration domain $\Omega_{\rm out}$ depends on Σ, since Σ is (part of) its boundary, while, as before, the distance function d depends on Σ too.

Another feature of the objective function (30) is the absence of a surface integral on Σ, contrary to the previous ones (15) and (28). The reason is that such a term would not be shape-differentiable. Indeed, as is clear from (22), the shape derivative of this surface integral would involve the value of the distance derivative d' on Σ, which does not make any sense since, in view of (17), d' is discontinuous on Σ. This absence of a surface integral is not a difficulty for our accessibility problems as explained below in Remark 5.4.

By the chain rule lemma, the computation of the shape derivative of (30) is a rather simple generalization of Propositions 4.4 and 5.1. Since the objective function (30) is different from (15), the adjoint equation has to be changed accordingly. The adjoint p is now a solution of

$$\left\{\begin{array}{rcll} -\mathrm{div}\,(V_+ p_+ \nabla d_+) &=& j'(d_+) & \text{in } \Omega_+, \\ -\mathrm{div}\,(V_- p_- \nabla d_-) &=& 0 & \text{in } \Omega_-, \\ p_+ &=& 0 & \text{on } \Gamma_c = \partial\Omega \setminus \Gamma_D, \\ V_+ p_+ \nabla d_+ \cdot n &=& V_- p_- \nabla d_- \cdot n & \text{on } \Sigma. \end{array}\right. \tag{31}$$

Proposition 5.3. *The objective function (30) is shape differentiable and its derivative, for any $\theta \in W^{1,\infty}(\Omega;\mathbb{R}^d)$, is given by*

$$\langle J'(\Sigma), \theta\rangle = \int_\Sigma \Big(V_+ \nabla d_+ \cdot n_+ p_+ n \cdot (\nabla d_+ - \nabla d_-) - j(d)\Big)\theta \cdot n\, ds, \tag{32}$$

with d_+, d_-, the solution of (7), and p_+ the adjoint state, solution of (31). Moreover, n_+, respectively n_-, is the outer unit normal vector to Ω_+, respectively Ω_-, and we choose $n = n_-$ as the normal vector to Σ.

Proof. The proof is completely similar to that of Proposition 4.4. The Dirichlet boundary condition for the adjoint p is homogeneous since there is no surface integral in the objective function (30). □

Remark 5.4. Although the objective function (30) does not feature an integral on Σ, it is possible to use if for detecting the normal accessibility of Σ when the integrand $j(d)$ is replaced by $h_\varepsilon(d - d_0)$, as defined in Subsection 3.1. Indeed, if $J(\Sigma) = 0$, then $h_\varepsilon(d - d_0) = 0$ in Ω_+ and by continuity $d - d_0 = 0$ on the interface Σ. Conversely, if $d - d_0 = 0$ on the interface Σ, then, restricting the eikonal equations (5) and (7) to Ω_+, where they have the same speed V_+, the solutions d and d_0 coincide on Ω_+. As we shall see in Section 9 this approach works nicely in numerical practice.

Remark 5.5. Propositions 5.1 and 5.3 are concerned with the notion of normal accessibility since the distance function, involved in the objective functions (28) and (30), is a solution of (7). Obviously similar results hold true for the notion of multidirectional accessibility, replacing the integrands $j(d)$ and $k(d)$ in the objective functions by $j(d_{y_1}, \ldots, d_{y_{N_y}})$ and $k(d_{y_1}, \ldots, d_{y_{N_y}})$, respectively, as in (25), where $(d_{y_1}, \ldots, d_{y_{N_y}})$ is the family of solutions of (8).

6. Mechanical model

6.1. Setting of the problem

In this subsection a linear elasticity model is introduced for the obstacle Ω_-, which is considered as a structure, while Ω_+ is a void space in the fixed domain Ω. Let $\Gamma_{N_{\mathrm{mec}}}$ and $\Gamma_{D_{\mathrm{mec}}}$ be two fixed disjoint subsets of the boundary $\partial\Omega$. In the previous sections the obstacle Ω_- was assumed (for simplicity) to be contained strictly inside Ω and its boundary was precisely $\Sigma = \partial\Omega_-$. Now, for the mechanical problem, this assumption must be dropped. On the contrary, the structure Ω_- has to touch the boundaries of the domain Ω because it is on $\Gamma_{N_{\mathrm{mec}}}$ that the loads are applied and on $\Gamma_{D_{\mathrm{mec}}}$ that it is clamped. Therefore, from now on, Σ is not equal to the entire boundary $\partial\Omega_-$ anymore but it reduces to the free boundary subset of $\partial\Omega_-$. In other words, the boundary of Ω_- is divided in three parts

$$\partial\Omega_- = \Gamma_{N_{\mathrm{mec}}} \cup \Gamma_{D_{\mathrm{mec}}} \cup \Sigma, \tag{33}$$

where $\Gamma_{N_{\mathrm{mec}}}$ is the part where the loading is applied, $\Gamma_{D_{\mathrm{mec}}}$ is the part where Ω_- is clamped and Σ is the rest of the boundary which is free (see Fig. 13). The set of admissible obstacle/structure Ω_- is defined as

$$\mathcal{U}_{ad} = \{\Omega_- \subset \Omega \text{ such that } \Gamma_{N_{\mathrm{mec}}} \cup \Gamma_{D_{\mathrm{mec}}} \subset \partial\Omega_-\}. \tag{34}$$

Since $\Gamma_{N_{\mathrm{mec}}}$ and $\Gamma_{D_{\mathrm{mec}}}$ are fixed and only Σ is subject to optimization, any admissible shape Ω_- is characterized by its free boundary Σ.

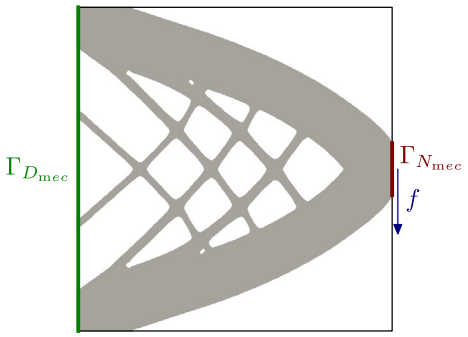

Fig. 13. The structure Ω_- with its boundaries and loads for the elasticity system (35).

For a given load $f \in L^2(\Gamma_{N_{\text{mec}}})^d$ consider the linearized elasticity problem

$$\begin{cases} -\text{div}\,(Ae(u)) = 0 & \text{in } \Omega_-, \\ Ae(u)n = f & \text{on } \Gamma_{N_{\text{mec}}}, \\ Ae(u)n = 0 & \text{on } \Sigma, \\ u = 0 & \text{on } \Gamma_{D_{\text{mec}}}, \end{cases} \tag{35}$$

where, as usual, $e(u) = \frac{1}{2}(\nabla u + \nabla u^T)$ is the strain tensor of the elastic displacement u and A is the uniform isotropic Hooke's law of the material occupying Ω_-. There exists a unique solution u in $H^1(\Omega_-)^d$ of (35). A classical problem of shape and topology optimization for Ω_- is to minimize its compliance under a volume constraint. The compliance for (35) is defined by

$$C(\Sigma) = \int_{\Gamma_{N_{\text{mec}}}} f \cdot u \, ds. \tag{36}$$

Note that the compliance of Ω_- is written as a function of Σ since this free boundary completely determines Ω_- by virtue of (33).

To compute the shape derivative of (36) we rely again on Hadamard method (see [5], [25]). However, since the shape Ω_- is constrained to stay inside the fixed domain Ω and its boundaries $\Gamma_{N_{\text{mec}}}$ and $\Gamma_{D_{\text{mec}}}$ are fixed subsets of the outer boundary $\partial\Omega$, we consider variations of the type $\Omega_{-\theta} = (Id + \theta)\Omega_-$ where the vector field $\theta \in W^{1,\infty}(\Omega; \mathbb{R}^d)$ vanishes on $\Gamma_{N_{\text{mec}}} \cup \Gamma_{D_{\text{mec}}}$ and its normal component vanishes on the whole $\partial\Omega$. Let us recall the following classical result [5,8].

Proposition 6.1. *The compliance $C(\Sigma)$, defined by (36), is shape differentiable and its derivative is written, for any $\theta \in W^{1,\infty}(\Omega, \mathbb{R}^d)$,*

$$C'(\Sigma)(\theta) = -\int_{\Sigma} \theta \cdot n \, Ae(u) : e(u) \, ds. \tag{37}$$

6.2. Coupled optimization

Finally this subsection defines one of the main optimization problems of this work: it is a coupled optimization for the accessibility and the compliance of the obstacle/structure Ω_-. As in Subsection 5.2, Ω_- is not only the obstacle, but its free boundary Σ is also the target surface where accessibility is measured. The compliance of Ω_- is also optimized in the same setting as that described in the previous subsection.

Although it is possible to start this optimization process from any initial design, we found it very convenient, in terms of problem formulation, and efficient, in terms of resulting designs, to initialize the optimization with a reference design Ω_-^{ref} which is obtained by minimizing the sole compliance with a volume constraint (thus, without any accessibility constraint). The free boundary of the reference shape Ω_-^{ref} is denoted by Σ^{ref}.

Let $J(\Sigma)$ be the accessibility criterion defined by (30). Recall that Σ and Ω_- are unambiguously related by (33). The goal is to optimize Ω_-, namely making it accessible, starting from Ω_-^{ref}, keeping its same volume, denoted by $|\Omega_-|$, while preserving as much as possible its compliance $C(\Sigma)$. To do so, introducing a small tolerance parameter $k \geq 0$ for the compliance constraint, we define the coupled optimization as

$$\begin{array}{rlll} \min\limits_{\Sigma \subset \Omega} & J(\Sigma) & & \\ \text{such that} & |\Omega_-| & = & |\Omega_-^{\text{ref}}| \\ & C(\Sigma) & \leq & (1+k)C(\Sigma^{\text{ref}}) \end{array} \tag{38}$$

where Ω_-, defined by Σ, belongs to $\mathcal{U}_{ad}$. Of course, the ultimate goal is to finish with a zero-value for the minimum of $J(\Sigma)$, with the smallest possible value of k, i.e., the least possible reduction of the mechanical performance.

7. Numerical algorithms

This section describes the numerical algorithms which are used in our test cases. The finite element analysis is performed with the open-source software FreeFEM [24]. On the other hand, the eikonal or Hamilton-Jacobi equations for the distance functions, as well as their adjoint equations, which are linear transport equations, are implemented in Python. Data exchanges between the two software are done by reading input files and writing output files, which is notably ineffective. Nevertheless, these two software are very convenient for their respective use and their coupling is straightforward. We leave to future work a more efficient implementation in a single unified code.

7.1. Eikonal and adjoint equations

In this subsection we explain how the eikonal or Hamilton-Jacobi equations (7) and (8) (the solutions of which are signed distance functions) and the adjoint equations (20) and (26) (which are necessary to evaluate the shape gradients) are solved numerically. For simplicity, we choose to solve them by using standard finite difference schemes on a cartesian mesh in Python. Of course, there are other possible algorithms and software packages, including some for unstructured meshes (see e.g. [14], [16]).

For solving the Hamilton-Jacobi equations (7) and (8), we rely on the Python extension module `scikit-fmm` [19] which implements the fast marching method. Another (slower) possibility is to use a standard upwind second-order finite difference scheme [37] for their time-dependent version and stop when a steady state is reached.

The adjoint equations (20) and (26) are linear transport equations with a transmission condition at the interface Σ. Because of this interface condition, the adjoint solutions p and p_{y_i} are not continuous through Σ but it is not a problem because the vector fields $Vp\nabla d$ and $Vp_{y_i}\nabla d_{y_i}$ have a continuous normal component through Σ. Therefore, these vector fields admit a well-defined divergence in the complete domain Ω and there is no special difficulty in the discretization of the transmission condition at the interface Σ. Thus, we solve a time-dependent version of (20) or (26) and wait for steady state to deduce a solution of (20) or (26). We use a standard first-order upwind scheme. An example of a numerical solution of the adjoint equation (20) was already shown in Fig. 10.

7.2. Level set method

In order to parametrize the obstacle Ω_- in a fixed computational mesh of the domain Ω, the level set method is used [36]. The obstacle Ω_- is defined by a level set function $\varphi : \Omega \to \mathbb{R}$ satisfying

$$\begin{cases} \varphi(x) = 0 & \text{if } x \in \Sigma, \\ \varphi(x) < 0 & \text{if } x \in \Omega_-, \\ \varphi(x) > 0 & \text{if } x \in \Omega_+. \end{cases}$$

Given $\mathcal{V}$ a scalar normal velocity, deduced from the shape derivative (see the next subsection), the level set function is updated by solving the following Hamilton-Jacobi equation, or transport equation:

$$\frac{\partial \varphi}{\partial t} + \mathcal{V}|\nabla \varphi| = 0 \quad \text{in } \Omega. \tag{39}$$

The solution of (39) is computed by solving the linearization of (39) with the method of characteristics [14] (more precisely, we rely on the software Advect from the ISCD Toolbox [16]). The mesh for solving (39) is the same as the one in Subsection 7.1. The level set function obtained after this advection step may not be equal to a signed function anymore. Thus, a redistancing procedure is performed at each iteration with the *distance* function in FreeFEM [24] (based on a fast marching algorithm [37]) so that the level set function φ remains the signed distance function to the actual shape. For more details on this all process, which is by now classical, we refer to [5].

7.3. Finite element solver for the mechanical equations

The linearized elasticity system (35) is numerically solved by the finite element method with FreeFEM [24]. Piecewise linear $\mathbb{P}_1$ finite elements on simplicial meshes are used. The extension-regularization process for the shape derivative, described in the next subsection, is also solved using FreeFEM. The optimization loop is managed by FreeFEM too. Only the eikonal and adjoint equations are solved by Python, as explained in Subsection 7.1.

It is classical when using the level set method for structural topology optimization [8], [5], to replace the elasticity system (35), posed in the sole structure Ω_-, by a similar elasticity system, posed in the whole computational domain Ω, where the void subdomain Ω_+ is filled with a weak "ersatz" material. In all our numerical examples, this weak ersatz material is taken as $10^{-3}A$, where A is the elasticity tensor of the isotropic material in the structure Ω_-. As explained in [8], [5], the overall elasticity tensor $A^*(x)$ in Ω is deduced from the sign of the level set function $\varphi(x)$, applying a volume averaging in the mesh cells cut by the zero level set of φ.

7.4. Extension and regularization of the shape derivative

We now explain how a scalar normal velocity field $\mathcal{V}(x)$, defined in the full domain Ω, can be deduced from the notion of shape derivative. It is obtained through a classical extension and regularization process [8], [5]. Recall that, for any (smooth) objective function $J(\Sigma)$, its shape derivative reads, for $\theta \in W^{1,\infty}(\Omega, \mathbb{R}^d)$,

$$J'(\Sigma)(\theta) = \int_\Sigma j\,\theta \cdot n\,ds,$$

where $j(x)$ depends on the solutions of some direct and adjoint problems. In principle, the choice $\theta = -jn$ yields a descent direction to decrease the objective function. However, the integrand j and the normal vector n are defined only on the interface Σ, while in numerical practice the velocity field θ should be known everywhere in the domain Ω. Since the level set method already gives an extension of the normal n, it remains to extend the scalar field j and to regularize it for a better convergence of the gradient algorithm. The extension $\mathcal{V} \in H^1(\Omega)$ of j is defined as the unique solution of the variational formulation

$$\int_\Omega (\varepsilon^2 \nabla\mathcal{V} \cdot \nabla W + \mathcal{V} W)\,dx = \int_\Sigma jW\,ds \quad \text{for all } W \in H^1(\Omega), \tag{40}$$

where the regularization parameter $\varepsilon > 0$ is typically the mesh size. Eventually, $\theta = -\mathcal{V}n$ guarantees a descent direction such that $J'(\Sigma)(-\mathcal{V}n) \le 0$ because of (40) with the choice $W = \mathcal{V}$.

To compute the integral on Σ in (40), since Σ is not exactly meshed, we rely on the *levelset* option for surface integrals in FreeFEM [24], which gives the possibility of integrating on a given levelset of a function. The integrand of the shape derivative involves a jump of the distance gradients (see (21) in Proposition 4.4) which is not easy to evaluate since Σ is not exactly meshed. A first approach amounts to extend ∇d_+ outside of Ω_+, respectively ∇d_- outside of Ω_-, by continuity, then to evaluate the jump on Σ. The implementation on a regular grid in Python is not excessively difficult but cannot easily be extended to unstructured meshes. Therefore we do not describe it in details. Rather, we advocate a second approach, relying on the formula in Corollary 4.7: the computation of jumps is circumvented by using Snell's law.

7.5. Gradient algorithm

The optimization problem (38) features two constraints: one equality constraint for the volume and an inequality constraint for the compliance. The volume constraint is exactly taken into account by the following projection process. After advecting the level set function by solving (39) at each optimization iteration, we add a constant c_{vol} to the level set function φ in order to satisfy the volume constraint. The precise value of c_{vol} is found by a simple dichotomy algorithm. For the compliance inequality constraint we rely on an augmented Lagrangian algorithm. Following [35] (section 17.4), and recalling that Ω_- depends on Σ, the augmented Lagrangian is written:

$$\begin{aligned}\mathcal{L}(\Sigma, \lambda, \mu) = J(\Sigma) \quad & -\lambda \max\left(C(\Sigma) - (1+k)C(\Sigma^{\text{ref}}), -\frac{\lambda}{\mu}\right) \\ & + \frac{\mu}{2}\left|\max\left(C(\Sigma) - (1+k)C(\Sigma^{\text{ref}}), -\frac{\lambda}{\mu}\right)\right|^2,\end{aligned} \tag{41}$$

where $\lambda \ge 0$ is the Lagrange multiplier for the compliance constraint, while $\mu > 0$ is the penalization coefficient. At each iteration j, the Lagrange multiplier λ is updated as:

$$\lambda^{j+1} = \lambda^j + \mu \max\left(C(\Sigma) - (1+k)C(\Sigma^{\text{ref}}), -\frac{\lambda}{\mu}\right),$$

while the shape derivative of the augmented Lagrangian $\mathcal{L}$ is used in the extension-regularization process of Subsection 7.4 to produce a velocity $\mathcal{V}_j$ which advects the interface Σ.

It is classical in the level set method for structural topology optimization [8], [5], that the equivalent of the descent step for the minimization of $\mathcal{L}$ is the final time of integration for the transport equation (39). For all our numerical test cases, this final time is chosen, at each iteration, as a typical mesh size divided by the maximal absolute value of the velocity $\mathcal{V}_j$. If the Lagrangian $\mathcal{L}$ does not decrease, the final time is divided by 2. On the contrary, if the Lagrangian $\mathcal{L}$ decreases, the final time (at the next iteration) is multiplied by a factor 1.1 to provide some adaptation and a faster convergence.

8. Geometric optimization test cases

This section is devoted to the optimization of accessibility criteria without any mechanical criterion. Therefore it is a purely geometric study. Recall that the volume constraint is enforced exactly at each iteration by updating the level set function accordingly. For all examples the obstacle velocity is taken as $V_- = 0.5$ (its precise value does not change the results significantly).

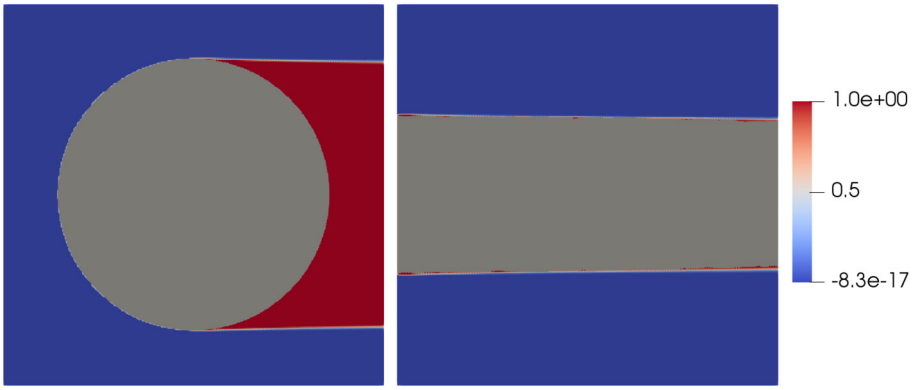

Fig. 14. Problem (42): plot of accessibility function $h_\varepsilon(d-d_0)$ for the initial shape (left) and optimized shape (right).

8.1. Optimization of the obstacle

We start by optimizing the obstacle Ω_-, using a gradient algorithm based on the shape derivatives established in Section 4. Recall that Ω_- is completely characterized by its boundary or interface Σ.

8.1.1. Normal accessibility

The first test case is the following minimization of a normal accessibility criterion under a volume constraint for the obstacle

$$\begin{aligned} &\min_{\Sigma\subset\Omega} && J_{1,\varepsilon}(\Sigma) \\ &\text{such that} && |\Omega_-| = |\Omega_-^{\text{ref}}| \end{aligned} \tag{42}$$

where $J_{1,\varepsilon}(\Sigma)$ is defined by (11). The purpose of the volume constraint is to avoid the disappearance of the obstacle when minimizing (42). The domain is a unit square $\Omega=(0,1)^2$. The target surface Γ_{out} is the right side of the square, while the starting surface Γ_D is the left side of the square. The initial shape Ω_-^{ref} of the obstacle is a disk of radius 0.22 centered in Ω. The value of ε is $h/10$, where $h=1/300$ is the mesh size. The computation is performed on a cartesian mesh with 300×300 nodes. The initial distance d and function $h_\varepsilon(d-d_0)$ were already displayed on Fig. 8. Because the obstacle satisfies a volume constraint, the target surface Γ_{out} cannot be normally accessible from Γ_D and, thus, the minimal value of (42) is strictly positive.

The result of the optimization is shown in Fig. 14 (right) with a plot of $h_\varepsilon(d-d_0)$. For comparison, on the left, the initial value of $h_\varepsilon(d-d_0)$ is also plotted (only the exterior domain Ω_+ is displayed). The shape obtained for the obstacle is close, but not exactly optimal for this problem. A rectangle as large as the domain with a minimal thickness to respect the volume constraint would perform better. The reason for this discrepancy is the slight "diffusion" of the shadow of the obstacle due to the regularized Heaviside function h_ε. The convergence is obtained after 175 iterations, each iteration requiring around 3 seconds of computation time (including solving (7) and (20), as well as the optimization steps). No effort has been made to improve the computational efficiency of our algorithm. Indeed, even in the present purely geometrical setting, we rely on the finite element software FreeFEM [24] for the optimization algorithm (extending the shape derivative by solving (40), advecting the level set function by solving (39)), while the eikonal and adjoint equations are solved within Python. The convergence for (42) is smooth as can be checked in Fig. 15.

8.1.2. Multi-directional accessibility

We now turn to the optimization of a multi-directional accessibility criterion under a volume constraint for the obstacle

$$\begin{aligned} &\min_{\Sigma\subset\Omega} && J_{2,\varepsilon}(\Sigma) \\ &\text{such that} && |\Omega_-| = |\Omega_-^{\text{ref}}| \end{aligned} \tag{43}$$

where $J_{2,\varepsilon}(\Sigma)$ is defined by (14). The definitions of Ω, Γ_{out} and Γ_D are the same as in the previous subsection. A cartesian mesh with 200×200 nodes is used. The regularization parameter of the Heaviside function is $\varepsilon=2/200$. The multi-directional accessibility is evaluated with only two points $(y_1,y_2)\in\Gamma_D$ which are placed at a distance 0.1 from the end points of Γ_D, with a radius $\epsilon=10^{-3/2}$, as shown in Fig. 16 (left, in yellow). The initial obstacle Ω_-^{ref} is an ellipsoidal shape, $3(x-1/2)^2+(y-1/2)^2\le 0.1$, as shown in Fig. 16 (left). The optimization process is the same as before, however its cost is double since there are two points (y_1,y_2) and the number of eikonal equations (2) and adjoint equations (26) is thus two, at each iteration. The optimized obstacle is shown in Fig. 16 (right).

The convergence history for the cost function (14) is shown in Fig. 17. Contrary to the test case of the previous subsection, the target surface Γ_{out} is accessible from the two points $y_1, y_2\in\Gamma_D$ and, thus, the minimal value of (43) is zero, as can

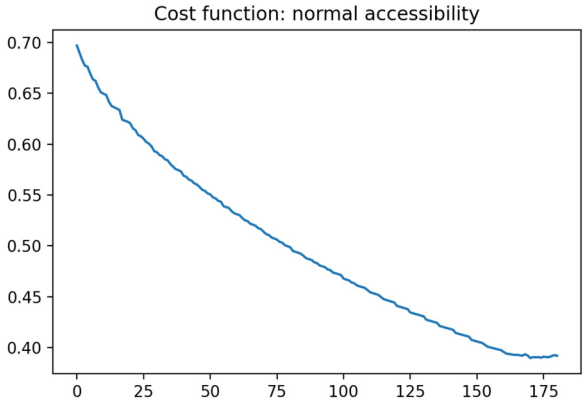

Fig. 15. Problem (42): convergence history for the criterion $J_{1,\varepsilon}(\Sigma)$.

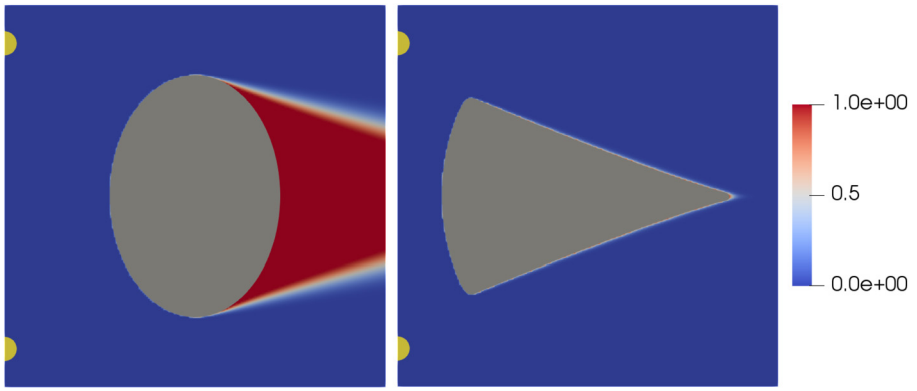

Fig. 16. Problem (43): plot of the integrand of $J_{2,\varepsilon}(\Sigma)$ for the initial shape (left) and final shape (right).

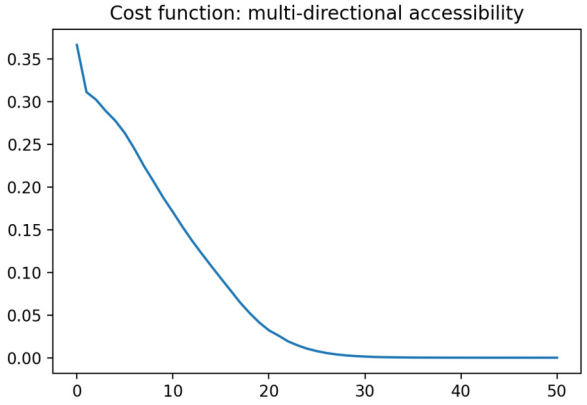

Fig. 17. Problem (43): convergence history for the criterion $J_{2,\varepsilon}(\Sigma)$.

be checked on Fig. 17. Note that there are many different optimal designs for problem (43). The one displayed on Fig. 16 (right) is just one example depending on the chosen initialization. In particular, the curved left boundary of the optimal design is inherited from the initialization but does not play any role in the optimality (a straight left boundary would be equally optimal, for example).

To explore further the uniqueness of solutions (or not) we performed another test for problem (43). The domain Ω is still the unit square but the two points y_1, y_2 are placed at the left corners with a radius $\epsilon = 10^{-3/2}$ and a finer 300×300 mesh. In such a case, neglecting terms of order ϵ, it is easy to build optimal solutions Ω_- of (43). If the initial shape Ω_-^{ref} has a volume less than 0.5, then the minimal value of (43) is zero and there are infinitely many optimal designs, including triangles with the left side of Ω as a base. If the volume $|\Omega_-^{\text{ref}}|$ is strictly larger than 0.5, then the minimal value of (43) is strictly positive and there are again infinitely many optimal designs, which are trapezoids supported by the left side and

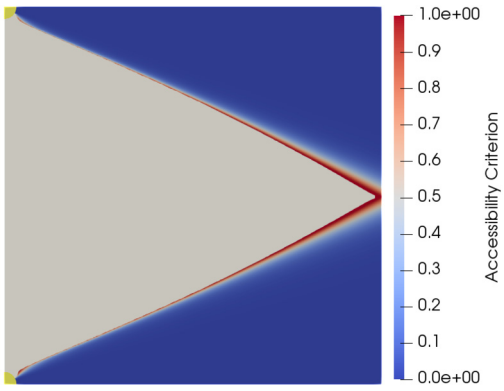

Fig. 18. Problem (43): plot of the integrand of $J_{2,\varepsilon}(\Sigma)$ for the optimal obstacle obtained with y_1, y_2 placed at the left corners and a volume constraint $|\Omega_-| = 0.5$.

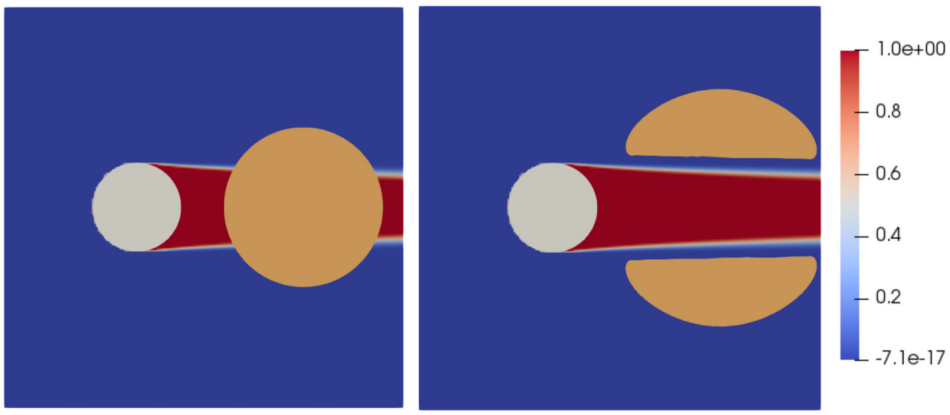

Fig. 19. Problem (44): initial shape of the target surface (left) and optimized one (right).

touching the right side of the square. The interesting case is $|\Omega_-^{\text{ref}}| = 0.5$, for which any optimal design is precisely a triangle (with base equal to the left side and touching the right side at one point), which is not unique, except if an horizontal symmetry is imposed. One such optimal triangle is displayed on Fig. 18: it is the unique symmetric optimal design. Note the effect of the numerical diffusion on the tip of the triangle (which is the reason we used a finer mesh).

8.2. Target surface optimization

We now optimize the shape of the subdomain Ω_{out}, the boundary of which is the target surface $\Gamma_{\text{out}} = \partial\Omega_{\text{out}}$. This is the setting of Section 5, where the shape derivatives were established. Only normal accessibility is considered here.

8.2.1. Fixed obstacle

We first assume that the obstacle Ω_- is fixed and does not vary during the optimization. The optimization problem is

$$\begin{aligned} &\min_{\Omega_{\text{out}} \subset \Omega} \quad J_{1,\varepsilon}(\Omega_{\text{out}}) = \int_{\partial\Omega_{\text{out}}} h_\varepsilon\,(d - d_0)\,ds \\ &\text{such that} \quad |\Omega_{\text{out}}| = |\Omega_{\text{out}}^{\text{ref}}|, \end{aligned} \tag{44}$$

where the objective function is identical to (11), except that it now depends on Ω_{out} and not on Σ which is fixed. The distance d is the solution of (7) and thus it does not depend on Ω_{out}. The domain is the square $\Omega = (0,1)^2$ and the starting surface Γ_D is the left side of the square. The obstacle Ω_- is a disk of radius 0.1 and center $(0.3, 0.5)$. The initial target surface $\Gamma_{\text{out}} = \partial\Omega_{\text{out}}$ is a circle of radius 0.2 and center $(0.7, 0.5)$. The mesh is of size 200×200 and the regularization parameter of the Heaviside function is $\varepsilon = 0.5/200$.

Fig. 19 displays the initial design (left) and the optimized one (right) together with the function $h_\varepsilon\,(d - d_0)$ which does not change through the iterations (since the obstacle Ω_- is fixed). As expected, the target domain Ω_{out} moves to avoid the shadow of the integrand $h_\varepsilon\,(d - d_0)$, yielding a zero value of the objective function and its gradient. The fixed obstacle Ω_- is plotted in white while the target domain Ω_{out} is orange. The convergence history of the criterion (44) is shown in Fig. 20.

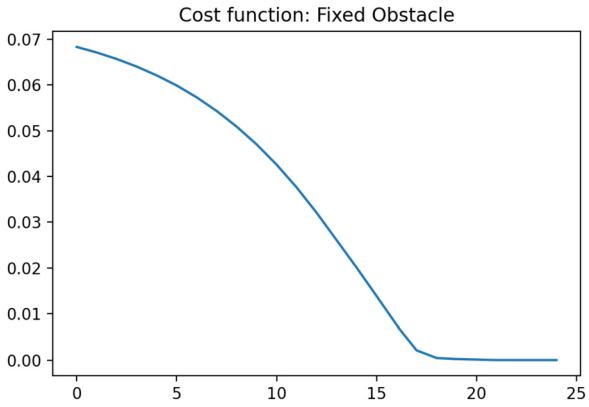

Fig. 20. Problem (44): convergence history for the objective function.

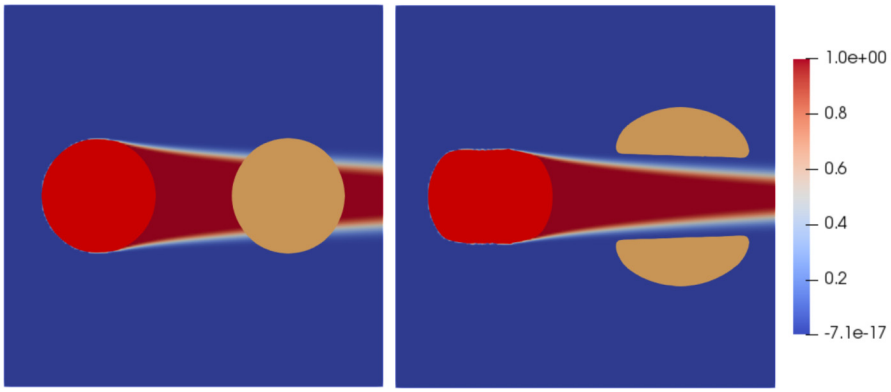

Fig. 21. Problem (45): initial shapes (left) and optimized ones (right).

8.2.2. Coupled optimization of the obstacle and target

In this subsection, the obstacle Ω_- and the target subdomain Ω_{out} are simultaneously optimized, a situation which is briefly discussed in Remark 5.2. The optimization problem under consideration is

$$\begin{array}{ll} \min\limits_{\Omega_-,\Omega_{\text{out}}\subset\Omega} & J_{1,\varepsilon}(\Sigma,\Omega_{\text{out}}) \\ \text{such that} & |\Omega_-| = |\Omega_-^{\text{ref}}|, \\ & |\Omega_{\text{out}}| = |\Omega_{\text{out}}^{\text{ref}}|, \end{array} \tag{45}$$

where Ω_-^{ref} and $\Omega_{\text{out}}^{\text{ref}}$ are the initial designs and

$$J_{1,\varepsilon}(\Sigma,\Omega_{\text{out}}) = \int_{\partial\Omega_{\text{out}}} h_\varepsilon\,(d-d_0)\,ds, \tag{46}$$

and d is the solution of (7). In other words, we want to normally access $\partial\Omega_{\text{out}}$ from the boundary Γ_D, optimizing both the obstacle Ω_- (or its boundary Σ) and the target Ω_{out}. In (45) there is a geometrical ambiguity: are the subdomains Ω_- and Ω_{out} disjoints or not? Both case are interesting but can possibly lead to different optimal designs. Here no constraint is imposed, meaning that they can intersect. However, in numerical practice, starting from well separated initial subdomains, they never get close and so they remain disjoint until convergence.

The same geometrical setting as in Subsection 8.2.1 is considered. The unit square Ω is discretized with a mesh of size 200×200 and the regularization parameter of the Heaviside function is $\varepsilon = 2/200$. The initial obstacle Ω_-^{ref} is a disk of radius 0.15 and center $(0.25, 0.5)$. The initial target surface $\Gamma_{\text{out}}^{\text{ref}} = \partial\Omega_{\text{out}}^{\text{ref}}$ is a circle of radius 0.15 and center $(0.75, 0.5)$. Since two different subdomains are optimized, two level set functions are required for tracking these two different optimization variables. This is a simple and well understood generalization of the setting presented in Subsection 7.2 and the reader is referred to [12] for details. The partial derivatives of $J_{1,\varepsilon}(\Sigma,\Omega_{\text{out}})$ are computed with Propositions 4.4 and 5.1. Fig. 21 displays the initial design (left) and the optimized one (right) together with the function $h_\varepsilon\,(d-d_0)$. The obstacle Ω_- is plotted in red while the target domain Ω_{out} is orange. The convergence history is shown in Fig. 22.

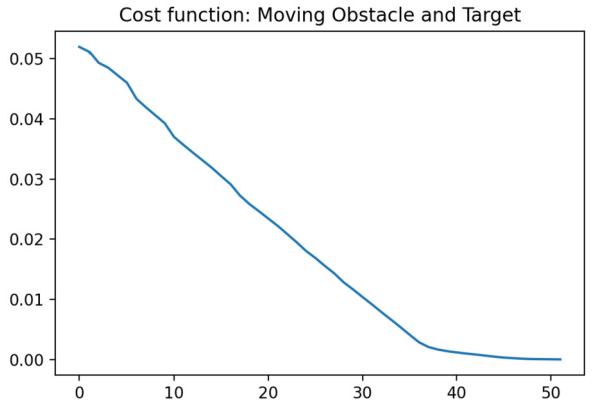

Fig. 22. Problem (45): convergence history for the criterion $J_{1,\varepsilon}(\Sigma, \Omega_{\text{out}})$.

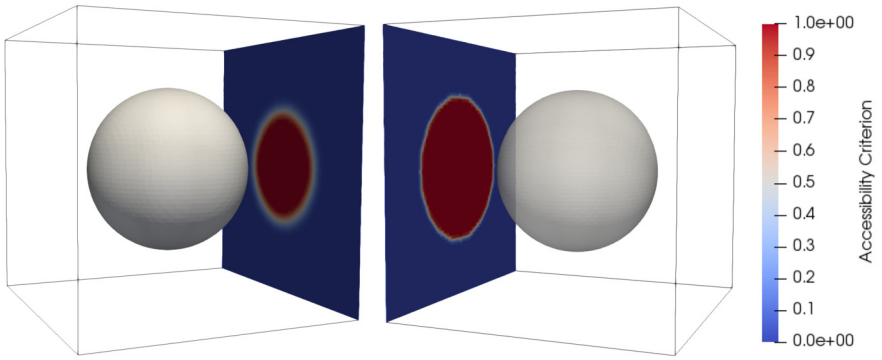

Fig. 23. Problem (42) in 3D: initial obstacle Ω_- with the plot of $h_\varepsilon(d - d_0)$ on Γ_{out} for high diffusion (left) and for low diffusion (right).

8.3. 3D optimization

8.3.1. Normal accessibility of the obstacle

As in Subsection 8.1.1 we solve the optimization problem (42) for a cubic domain $\Omega = (0,1)^3$. Normal accessibility is evaluated from the lower side Γ_D of the cube and the target surface Γ_{out} is the upper side. The initial obstacle is a sphere of radius 0.3, placed at the center of Ω and shown in Fig. 23. It turns out that, at least in 3D, the result is quite sensitive to the numerical diffusion which has two origins: first, the mesh size and, second, the regularization parameter ε of the Heaviside function h_ε. Therefore, we show the results for two different cases of high diffusion (coarser mesh of size $60 \times 60 \times 60$ with $\varepsilon = 1/60$ of the order of the mesh size) and of low diffusion (finer mesh of size $70 \times 70 \times 70$ with $\varepsilon = 0.1/70$, smaller than the mesh size)

In Fig. 23 the function $h_\varepsilon(d - d_0)$ is plotted on Γ_{out} for the initial shape Ω_-: clearly the shadow of the obstacle is smaller for high diffusion (left) than for low diffusion (right). The optimized obstacle is shown on Fig. 24: it is a cylinder (as expected) for low diffusion (right) but it has a kind of fractal shape for high diffusion (left) with almost no shadow. Indeed, numerical diffusion has a tendency to bend the rays and it is maximal at the interface Σ. Therefore, an oscillating or fractal interface induces a lot of diffusion and almost no shadow. The minimal values of the objective functions are completely different in the two cases as can be checked on Fig. 25. An iteration requires 1 minute of computation in the optimization process.

8.3.2. Coupled optimization of the obstacle and target

We now solve the optimization problem (45), extending to 3D the study of Subsection 8.2.2. The domain is a cube $\Omega = (0,1)^3$ (discretized by a $60 \times 60 \times 60$ grid) and normal accessibility is evaluated from one side of the cube Γ_D (defined by $x = 0$). The initial obstacle Ω_- is a sphere of radius 0.2 and center $(0.25, 0.5, 0.5)$, while the initial target Ω_{out} is a slab of thickness 0.2 and center $x = 0.75$, parallel to the side Γ_D, shown in Fig. 26. The regularization parameter of the Heaviside function is $\varepsilon = 0.5/60$. The optimized shapes are shown in Fig. 27 and the convergence history is displayed on Fig. 28. A hole has been created in the middle of the target Ω_{out} and the obstacle Ω_- has changed its shape to fit this hole.

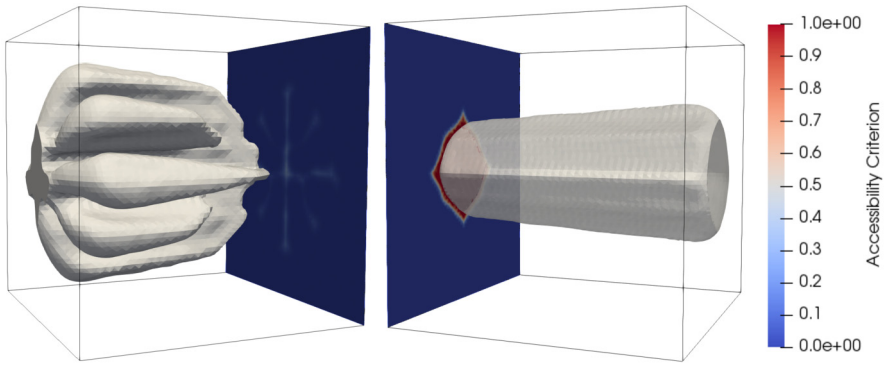

Fig. 24. Problem (42) in 3D: optimized obstacle Ω_- for high diffusion (left) and for low diffusion (right).

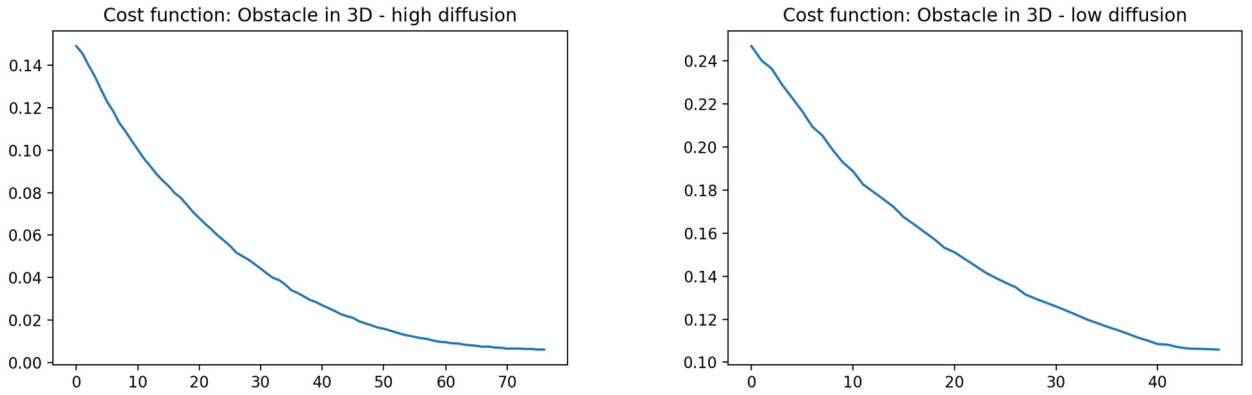

Fig. 25. Problem (42) in 3D: convergence histories for the criterion (11) with high diffusion (left) and low diffusion (right).

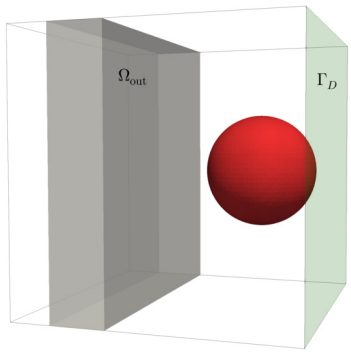

Fig. 26. Problem (45) in 3D: initial obstacle Ω_- (in red) and target Ω_{out} (in grey).

9. Mechanical optimization with accessibility

We now come to applications for structural optimization. In the sequel all volume constraints are enforced exactly at each iteration by updating the level set function accordingly (cf. Subsection 7.5).

9.1. 2D cantilever

Following the setting of Subsection 6.2 we first consider a coupled optimization problem for compliance minimization and accessibility satisfaction in 2D. The domain is the square $\Omega = (0,1)^2$. Its left and right sides are denoted by Γ_{D_1} and Γ_{D_2}, respectively. We work with the notion of normal accessibility, starting from one of the two lateral sides Γ_{D_1} or Γ_{D_2} (see Fig. 29, left). The structural shape is also the obstacle Ω_-. The accessibility criterion is measured on the complement $\Omega_+ = \Omega \setminus \Omega_-$ of the obstacle. Therefore, there is a single optimization variable which is the free boundary or interface Σ between Ω_- and Ω_+. The boundary conditions for the elasticity equations are those of Fig. 13, namely the Dirichlet

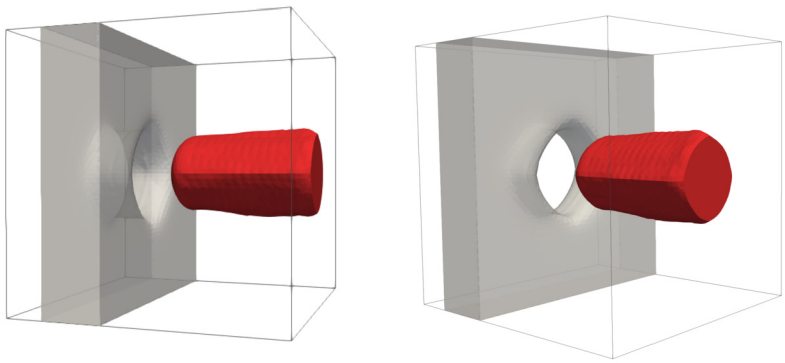

Fig. 27. Problem (45) in 3D: two views of the optimized obstacle Ω_- and target Ω_{out}.

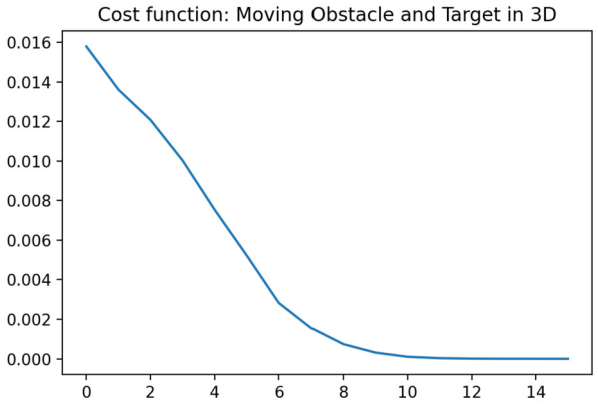

Fig. 28. Problem (45) in 3D: convergence history for $J_{1,\varepsilon}(\Sigma, \Omega_{\text{out}})$.

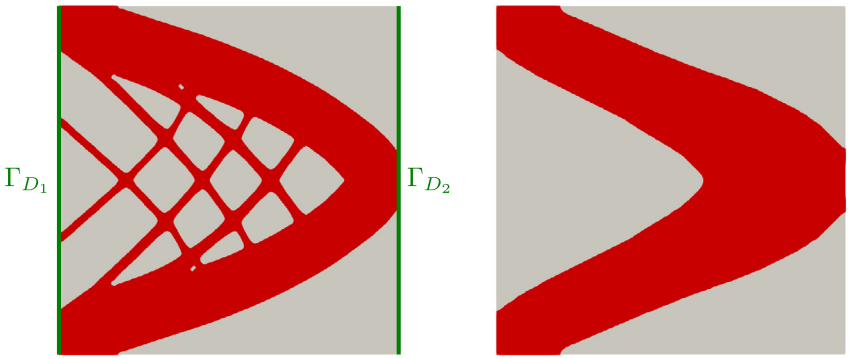

Fig. 29. Problem (47): initial reference shape Ω_-^{ref} (left) and optimized shape (right).

boundary is the left side, $\Gamma_{D_{\text{mec}}} = \Gamma_{D_1}$, the vertical surface force $f = (0, 1)$ is applied on the segment $(0.4; 0.6)$ inside the right side Γ_{D_2}, while the rest of the boundary of Ω is traction-free. The reference shape Ω_-^{ref} has a volume $|\Omega_-^{\text{ref}}| = 0.45|\Omega|$ and is plotted on the left of Fig. 29. The mesh in Ω has $40,000$ nodes. The Young modulus is $E = 1$ and the Poisson ratio is $\nu = 0.3$.

We consider the optimization problem (38) but with a slightly different objective function, namely

$$\begin{aligned} \min_{\Sigma \subset \Omega} \quad & J_3(\Sigma) \\ \text{such that} \quad & |\Omega_-| = |\Omega_-^{\text{ref}}| \\ & C(\Omega_-) \le (1+k) C(\Omega_-^{\text{ref}}), \end{aligned} \tag{47}$$

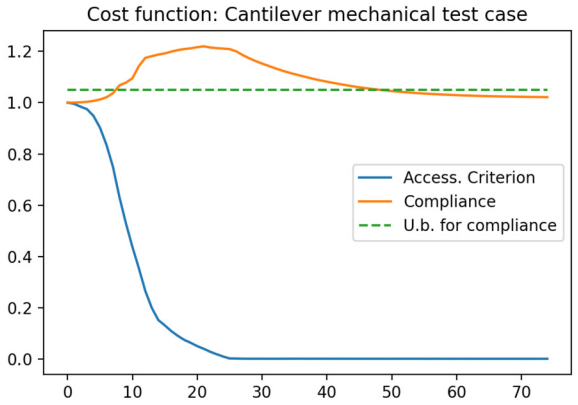

Fig. 30. Problem (47): convergence histories for the criterion $J_3(\Sigma)$ (blue) and the compliance (orange) with the upper bound for the compliance (dotted line).

where the tolerance is $k = 0.05$. The difference with (38) is that the normal accessibility is evaluated from one of the two sides Γ_{D_1} or Γ_{D_2}, separately, and not from their union $\Gamma_{D_1} \cup \Gamma_{D_2}$ (see Remark 9.1 below for an explanation). More precisely, the objective function is

$$J_3(\Sigma) = \int_{\Omega_+} h_\varepsilon \left(\min_{i=1,2} (d_i - d_{0,i}) \right) ds, \tag{48}$$

where each distance function d_i satisfies a Dirichlet boundary condition only on Γ_{D_i} and is a solution of

$$\begin{cases} V(x)|\nabla d_i(x)| &= 1 \quad \text{in } \Omega, \\ d_i &= 0 \quad \text{on } \Gamma_{D_i}, \end{cases} \tag{49}$$

where $V(x)$ is defined by (6) with $V_- = 0.5$ and $V_+ = 1$. Eventually, replacing $V(x)$ by the constant 1 in (49) yields the solution $d_{0,i}$. The shape derivative of the objective function (48) is given by a slight variant of Proposition 5.3, since there are two distance functions instead of just one. The derivative reads

$$\langle J_3'(\Sigma), \theta \rangle = \int_\Sigma \left(V_+ \sum_{i=1}^{2} \left(\nabla d_{i,+} \cdot n_+ p_{i,+} n \cdot (\nabla d_{i,+} - \nabla d_{i,-}) \right) + h_\varepsilon \left(\min_{i=1,2} (d_i - d_{0,i}) \right) \right) \theta \cdot n \, ds.$$

The optimized shape for problem (47) is displayed on Fig. 29 (right). Convergence histories for the criterion (48) and the compliance are shown in Fig. 30 (these quantities are normalized by their initial values). The volume constraint is enforced exactly at each iteration. The objective function $J_3(\Sigma)$ is initially not zero, meaning that the boundaries of the holes are not accessible, while its final value is zero, implying that the optimized shape is indeed accessible. During the optimization, the bars are first broken by the algorithm to make the free boundary Σ accessible. Then the classical shape of the short cantilever composed of two bars is found. This shape is optimized for the compliance while its free boundary is obviously normally accessible from the left or right side of the domain.

Remark 9.1. The reason for evaluating the objective function $J_3(\Sigma)$ with two distance functions (instead of just one with Dirichlet boundary condition on $\Gamma_{D_1} \cup \Gamma_{D_2}$) comes from the fact that Definition 2.3 of normal accessibility is not equivalent to the geometrical accessibility as already explained with the counter-example of Fig. 5. More precisely, satisfying the condition of Definition 2.3 implies geometrical accessibility but not the converse. However, as illustrated by the previous numerical example, the converse holds true in this case, when using two distance functions, one for each connected component Γ_{D_1} and Γ_{D_2}.

9.2. Accessibility problem for additive manufacturing

We turn to the main application of our accessibility constraint in the context of additive manufacturing. When building a mechanical structure ω by an additive manufacturing process like, e.g., selective laser melting (SLM) or laser powder bed fusion (LPBF), it is often necessary to mitigate the so-called overhang effects, the thermal deformations or residual stresses, by adding supports S to the structure. These supports allow the correct manufacturing of the structure and are removed after the process ends, since they are not necessary for the final use of the structure. Usually, these sacrificial supports are removed by a cutting tool, but it presupposes that the contact zone between the structure and the supports is accessible to the cutting tool. We model the accessibility constraint by Definition 2.3 of normal accessibility. Of course, the structure

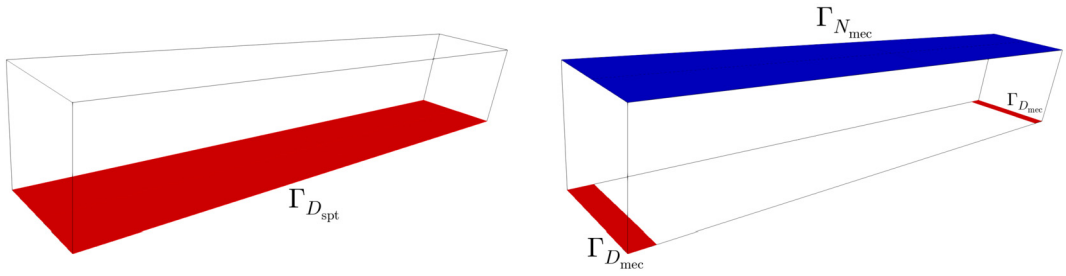

Fig. 31. Boundary conditions for the mechanical equations (50) (left) and (51) (right). The load for (50) (left) is a uniform vertical force applied in the structure ω, while the load for (51) (right) is a uniform vertical force applied on the blue top boundary.

ω is optimized for its final use while the support S is optimized for minimal weight, maximal efficiency and accessibility for its final removal. For the accessibility constraint the obstacle is $\Omega_- = \omega$. As before, the complete domain is Ω and the structure ω, as well as its supports S, must belong to Ω.

As mentioned before, there are two mechanical problems to consider. The first one is a model to evaluate the manufacturability of the couple structure-supports. There are several possible approaches to optimize supports, see e.g. [30], [34], [39]. Here, we follow the approach of [2] where the idea is to evaluate the rigidity of $\Omega_S = \omega \cup S$ under pseudo-gravity loads applied only in ω. More precisely we look for the unique solution $u_{\text{spt}} \in H^1(\Omega_S)^3$ of

$$\left\{\begin{array}{rcll} -\text{div}\,(Ae(u_{\text{spt}})) & = & g_\omega & \text{in } \Omega_S, \\ Ae(u_{\text{spt}})n & = & 0 & \text{on } \partial\Omega_S \setminus \Gamma_{D_{\text{spt}}}, \\ u_{\text{spt}} & = & 0 & \text{on } \Gamma_{D_{\text{spt}}}, \end{array}\right. \tag{50}$$

where g_ω is a constant unit vertical load applied downward in ω and not in S. The mechanical properties of the material inside ω and S are the same, so the isotropic Hooke's tensor A is constant in Ω_S.

The second problem describes the final-use of the sole structure ω. For a given surface load $f \in L^2(\Gamma_{N_{\text{mec}}})^3$, we look for the unique solution u_ω in $H^1(\omega)^3$ of

$$\left\{\begin{array}{rcll} -\text{div}\,(Ae(u_\omega)) & = & 0 & \text{in } \omega, \\ Ae(u_\omega)n & = & f & \text{on } \Gamma_{N_{\text{mec}}}, \\ Ae(u_\omega)n & = & 0 & \text{on } \partial\omega \setminus (\Gamma_{N_{\text{mec}}} \cup \Gamma_{D_{\text{mec}}}), \\ u_\omega & = & 0 & \text{on } \Gamma_{D_{\text{mec}}}. \end{array}\right. \tag{51}$$

Two compliances are computed for problems (50) and (51)

$$C_S(S,\omega) = \int_{\Omega_S} g_\omega \cdot u_{\text{spt}} dx \quad \text{and} \quad C_\omega(\omega) = \int_{\Gamma_{N_{\text{mec}}}} f \cdot u_\omega ds.$$

Minimizing $C_\omega(\omega)$ is a classical way of improving the rigidity of the structure ω for its final use, while minimizing $C_S(S,\omega)$ is one possible way of optimizing the placement of supports, helping to manufacture ω. For simplicity, the mechanical objective is just the sum of both compliances, denoted by

$$C(S,\omega) = C_S(S,\omega) + C_\omega(\omega).$$

Of course, it is possible to weight differently the two compliances C_S and C_ω, or equivalently to scale differently the two loads f and g_ω, or even to minimize one compliance with a constraint on the other. All these various choices would lead to possibly different optimal designs: nevertheless, the above objective function is enough for illustrating the effect of the proposed accessibility criterion on the final result. For comparison and initialization purposes, we first introduce a simpler problem, without any accessibility constraint, which reads

$$\begin{array}{ll} \min\limits_{\omega, S \subset \Omega} & C(\omega, S) \\ \text{such that} & |\omega| = V_\omega, \\ & |S| = V_S, \end{array} \tag{52}$$

for some given volume constraints V_ω, V_S. The optimal shapes for (52) will be the initial shapes $\omega_{\text{init}}, S_{\text{init}}$ for the following accessibility optimization. We rely on Definition 2.3 of normal accessibility from another part of the boundary, Γ_D, of the domain Ω. The part ω is considered as the obstacle Ω_- and accessibility is evaluated on S (disjoint from ω). The final optimization problem is thus

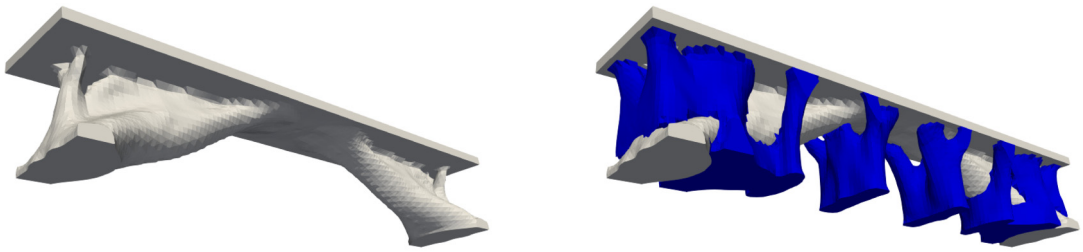

Fig. 32. Problem (52): optimized shapes of the bridge ω (white) and its supports S (blue).

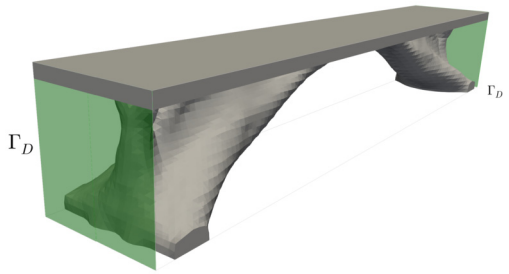

Fig. 33. Problem (53): boundary Γ_D from which normal accessibility is evaluated.

$$\begin{array}{ll} \min\limits_{\omega, S\subset\Omega} & J_3(\omega, S) \\ \text{such that} & |\omega| = |\omega_{\text{init}}|, \\ & |S| = |S_{\text{init}}|, \\ & C(\omega, S) \le (1+k)C(\omega_{\text{init}}, S_{\text{init}}), \end{array} \tag{53}$$

where $k > 0$ is a small tolerance and $J_3(\omega, S)$, very similarly to (48), is defined by

$$J_3(\omega, S) = \int_S h_\varepsilon\,(d - d_0)\,ds, \tag{54}$$

with the distance function d, solution of (7), which depends on the obstacle ω. The volume constraints in problems (52) and (53) are enforced exactly at each iteration. Since both ω and S are optimized, two level set functions, φ_ω and φ_S, are used as already explained in Subsection 8.2.2, one for each domain. For both mechanical problems (50) and (51) we rely on the ersatz material approach of Subsection 7.3. Since (51) does not involve the support S, the overall elasticity tensor A^* in the computational domain Ω is deduced solely from φ_ω, exactly as described in Subsection 7.3. However, (50) is posed in the union $\omega \cup S$: therefore, in this case, the overall elasticity tensor A^* in Ω is obtained from $\min(\varphi_\omega, \varphi_S)$, which is a level set function for $\omega \cup S$. Note that, by construction S and ω cannot overlap since the two level set functions are independent.

As a numerical example a bridge test case is studied. The domain Ω is a rectangular box $(-3, 3) \times (-0.5, 0.5) \times (0, 1)$, displayed with its different boundary conditions for equations (50) and (51) in Fig. 31. The Dirichlet boundary $\Gamma_{D_{\text{spt}}}$ for (50) is the baseplate or lower side $\{z = 0\}$. The Neumann boundary $\Gamma_{N_{\text{mec}}}$ for (51) is the road or upper side $\{z = 1\}$. The Dirichlet boundary $\Gamma_{D_{\text{mec}}}$ for (51) is made of the two extremities $\{|x| \le 2.8\}$ of the lower side $\{z = 0\}$. The boundary Γ_D for normal accessibility are the two lateral sides $\{x = \pm 3\}$, as shown in Fig. 33 (green). This choice of Γ_D is not completely meaningful from an engineering point of view (the other lateral sides could be taken into account for accessibility) but it makes the optimization more difficult and thus the test case more demanding and illustrative. To decrease the computational cost, two symmetries are applied with respect to the vertical symmetry planes in order to reduce the computational domain to one quarter of the initial domain: $(0, 3) \times (0, 0.5) \times (0, 1)$. This symmetry condition applies to both the mechanical equations and the eikonal equation for the distance function. Furthermore, to represent the road on top of the bridge a thin layer of elements on top of the rectangle is full of material and cannot be removed from the structure ω. The thickness of this non-optimizable layer is 0.1. The mesh of one fourth of the domain is of size $61 \times 11 \times 21$. The regularization parameter of the Heaviside function is $\varepsilon = 0.5/20$ since there are 20 mesh points per unit length. On top of this road a vertical unit force is applied, $f = (0, 0, -0.1)$ in (51). Solving problem (52) leads to the optimized shapes in Fig. 32 (after around 200 iterations). It is clear from the right picture in Fig. 32 that the support is not completely accessible along the normal direction from the lateral sides Γ_D.

Starting from the initial design $\omega_{\text{init}}, S_{\text{init}}$, obtained when solving (52), we now solve problem (53) allowing a relative increase in the compliance $k = 0.05$. The pseudo-gravity load in (53) is equal to $g_\omega = (0, 0, -2.5)$. The choice of the numerical parameters is made such that both compliances $C_\omega(\omega)$ and $C_S(S, \omega)$ are of comparable magnitudes for the given configuration. The resulting optimal shapes and topologies are shown in Fig. 34. Note the dramatic change, not only on the

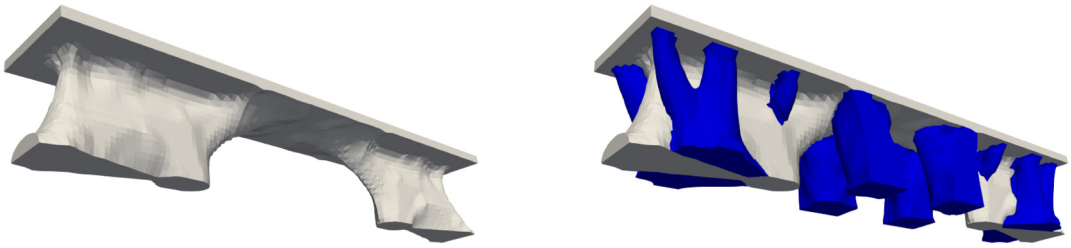

Fig. 34. Problem (53): optimized shapes of the bridge ω (white) and its supports S (blue).

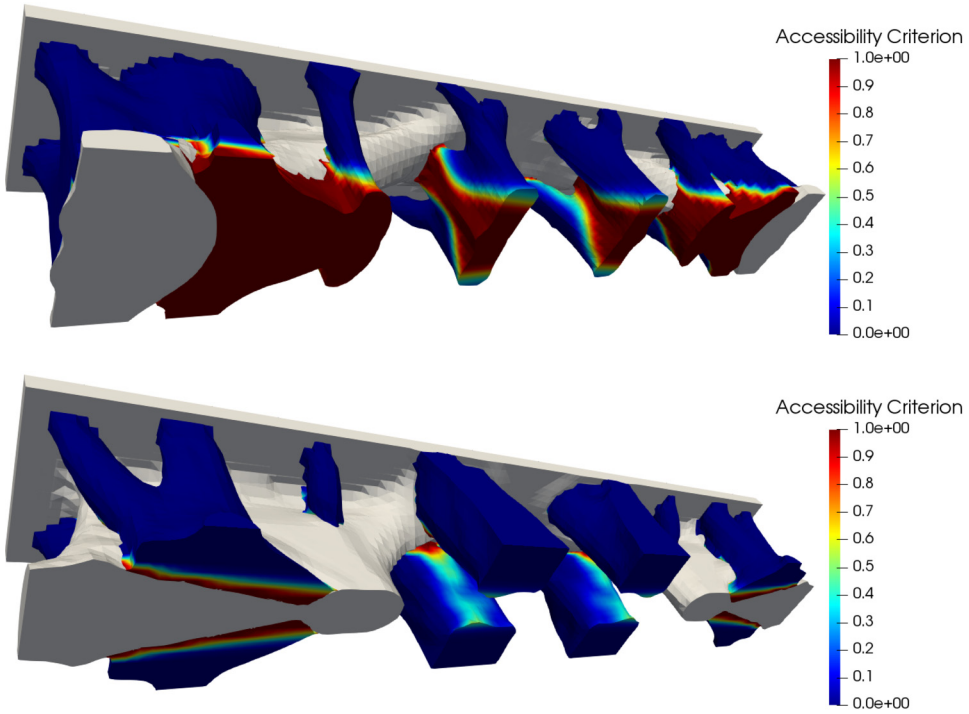

Fig. 35. Problem (53): integrand $h_\varepsilon(d - d_0)$ of the accessibility function (54) for the initialization (top) and the optimized design (bottom).

support S, but also in the bridge ω. The accessibility criteria is not exactly zero but it has decreased by 85%. Therefore the support S is now almost entirely accessible from the lateral sides Γ_D, as one can check on Fig. 35 where the integrand $h_\varepsilon(d - d_0)$ of the accessibility objective function (54) is plotted. It is mostly the lower part of the support, close to the baseplate $\Gamma_{D_{\text{spt}}}$, which is not completely accessible after optimization. Convergence histories of the objective and constraints are gathered in Fig. 36.

Remark 9.2. The objective function $J_3(\omega, S)$ is evaluated in the setting of Definition 2.3 of normal accessibility which is a simplified and stricter criterion for accessibility, compared to Definition 2.1 of multi-directional accessibility. Our choice of normal accessibility versus multi-directional accessibility is dictated only by CPU savings. Its drawback is that the objective function does not vanish at convergence (see Fig. 36) while it would be smaller with multi-directional accessibility and perhaps even vanishing.

Moreover, in problem (53) involving the criterion (54), the accessibility of the whole volume of the supports is considered. More refined criteria involving only the contact regions of the support with the structure ω and the baseplate could be considered.

10. Conclusion and perspectives

We introduced two notions of accessibility (normal or multi-directional) of a target surface from a starting surface, avoiding an obstacle. One advantage is that these definitions are amenable to shape optimization. We showed on several numerical examples in 2D and 3D that the proposed approach is indeed effective. In particular, it can be coupled with a problem of structural optimization and it turns out to be very useful for support optimization in the context of additive

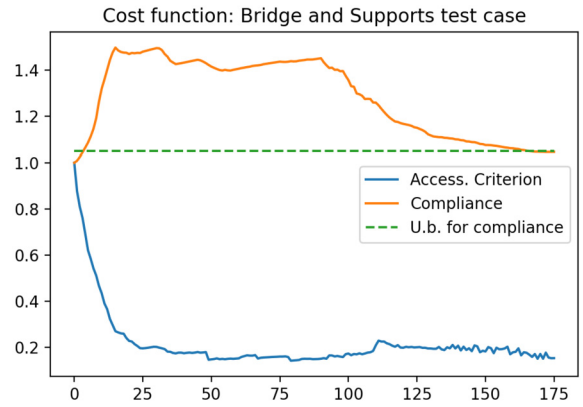

Fig. 36. Problem (53): convergence histoires for the sum of compliances $C(\omega, S)$ (orange) and the accessibility criterion (54) (blue).

manufacturing. Taking into account such an accessibility constraint guarantees that the supports can be removed by a cutting tool after the fabrication process.

There remain several issues to address. From the theoretical side one should prove that the adjoint equations (20) and (26) are well-posed which is not obvious since they are transport equations with non-smooth vector fields. Since they are under conservative forms, there is some hope to rigorously analyse them thanks to the theory in [13,26]. This is work in progress and is a key ingredient for rigorously justifying the formulas of the shape derivatives. From the numerical side, more testing of the multi-directional accessibility criterion should be done and its computational cost could be improved. Handling a sharp interface with a discontinuous velocity is not very efficient when the mesh does not fit the interface. In the spirit of [3] one could rely on a diffuse interface model (still based on signed distance functions) which would have the advantage of leading to smoother adjoints and shape derivatives. Alternatively, one could use the level set method in a body-fitted mesh setting, as explained in [5].

Of course, the proposed accessibility constraint can be coupled with more complex mechanical problems than just compliance minimization, not to mention other applications beyond structural mechanics. Finally, our notion of accessibility could be generalized. For the moment, it is based on a simple straight line connecting one point from the starting surface to one point in the target surface without touching the boundary. One could replace this line by a tube of fixed radius, which makes the criterion more realistic, although tighter.

Declaration of competing interest

The authors declare the following financial interests/personal relationships which may be considered as potential competing interests:
Gregoire Allaire reports financial support was provided by Public Investment Bank, France. Martin Bihr reports financial support was provided by National Association of Technical Research.

Data availability

No data was used for the research described in the article.

Acknowledgements

This work was partially supported by the SOFIA project, funded by BPI (Banque Publique d'Investissement). This work originates from the PhD thesis of M. Bihr which was supported by the Association Nationale de la Recherche et de la Technologie (ANRT), grant number CIFRE 2018/1405.

References

[1] G. Allaire, M. Bihr, B. Bogosel, Support optimization in additive manufacturing for geometric and thermo-mechanical constraints, Struct. Multidiscip. Optim. 61 (2020) 2377–2399.
[2] G. Allaire, B. Bogosel, Optimizing supports for additive manufacturing, Struct. Multidiscip. Optim. 58 (6) (Dec. 2018) 2493–2515.
[3] G. Allaire, C. Dapogny, G. Delgado, G. Michailidis, Multi-phase structural optimization via a level set method, ESAIM Control Optim. Calc. Var. 20 (2014) 576–611.
[4] G. Allaire, C. Dapogny, R. Estevez, A. Faure, G. Michailidis, Structural optimization under overhang constraints imposed by additive manufacturing technologies, J. Comput. Phys. 351 (2017) 295–328.
[5] G. Allaire, C. Dapogny, F. Jouve, Shape and topology optimization, in: Geometric Partial Differential Equations, Part 2, Elsevier/North Holland, Amsterdam, 2021, pp. 1–132.

[6] G. Allaire, F. Jouve, G. Michailidis, Molding direction constraints in structural optimization via a level-set method, in: Variational Analysis and Aerospace Engineering, Mathematical Challenges for the Aerospace of the Future, vol. 116, Springer Optimization and Its Applications, 2016, pp. 1–39.
[7] G. Allaire, F. Jouve, G. Michailidis, Thickness control in structural optimization via a level set method, Struct. Multidiscip. Optim. 53 (6) (2016) 1349–1382.
[8] G. Allaire, F. Jouve, A.-M. Toader, Structural optimization using sensitivity analysis and a level-set method, J. Comput. Phys. 194 (1) (2004) 363–393.
[9] L. Ambrosio, Lecture notes on geometric evolution problems, distance function and viscosity solutions, in: G. Buttazo, A. Marino, M.K.V. Murthy (Eds.), Calculus of Variations and Partial Differential Equations. Topics on Geometrical Evolution Problems and Degree Theory, 1999, pp. 5–93.
[10] L. Ambrosio, Transport equation and Cauchy problem for BV vector fields, Invent. Math. 158 (2) (2004) 227–260.
[11] G. Barles, Solution de viscosité des équations de Hamilton-Jacobi, Springer-Verlag, 1994.
[12] M. Bihr, Optimisation Topologique du Couple Pièce/Support pour la Fabrication Additive sur Lit de Poudre, PhD thesis, Institut Polytechnique de Paris, Dec. 2021, https://tel.archives-ouvertes.fr/tel-03631143.
[13] F. Bouchut, F. James, One-dimensional transport equations with discontinuous coefficients, Nonlinear Anal., Theory Methods Appl. 32 (7) (1998) 891–933.
[14] C. Bui, C. Dapogny, P. Frey, An accurate anisotropic adaptation method for solving the level set advection equation, Int. J. Numer. Methods Fluids 70 (7) (2012) 899–922.
[15] S. Cacace, E. Cristiani, L. Rocchi, A level set based method for fixing overhangs in 3d printing, Appl. Math. Model. 44 (2017) 446–455.
[16] C. Dapogny, P. Frey, A. Froelhy, ISCD toolbox, https://github.com/ISCDtoolbox, 2019.
[17] M. Delfour, J.-P. Zolésio, Shapes and Geometries, Advances in Design and Control, vol. 4, Society for Industrial and Applied Mathematics (SIAM), Philadelphia, PA, 2001.
[18] M.C. Delfour, J.-P. Zolésio, Shape identification via metrics constructed from the oriented distance function, Control Cybern. 34 (2005) 137–164.
[19] J. Furtney, scikit-fmm, https://pythonhosted.org/scikit-fmm/. (Accessed 14 November 2022).
[20] R. Glowinski, Numerical simulation for some applied problems originating from continuum mechanics, in: Trends in Applications of Pure Mathematics to Mechanics, Symp., Palaiseau/France 1983, in: Lecture Notes in Physics, vol. 195, Springer, 1984, pp. 96–145.
[21] J. Guest, Imposing maximum length scale in topology optimization, Struct. Multidiscip. Optim. 37 (5) (2009) 463–473.
[22] J.K. Guest, J.H. Prévost, T. Belytschko, Achieving minimum length scale in topology optimization using nodal design variables and projection functions, Int. J. Numer. Methods Eng. 61 (2) (2004) 238–254.
[23] X. Guo, W. Zhang, W. Zhong, Explicit feature control in structural topology optimization via level set method, Comput. Methods Appl. Mech. Eng. 272 (2014) 354–378.
[24] F. Hecht, New development in freefem++, J. Numer. Math. 20 (3–4) (2012) 251–266.
[25] A. Henrot, M. Pierre, Shape Variation and Optimization. A Geometrical Analysis, vol. 28, European Mathematical Society (EMS), Zürich, 2018.
[26] F. James, F. Bouchut, S. Mancini, Uniqueness and weak stability for multi-dimensional transport equations with one-sided Lipschitz coefficient, Ann. Sc. Norm. Super. Pisa, Cl. Sci. (5) 4 (1) (2005) 1–25.
[27] Z. Jihong, Z. Han, W. Chuang, Z. Lu, Y. Shangqin, W. Zhang, A review of topology optimization for additive manufacturing: status and challenges, Chin. J. Aeronaut. 34 (1) (2021) 91–110.
[28] M. Langelaar, An additive manufacturing filter for topology optimization of print-ready designs, Struct. Multidiscip. Optim. 55 (2016) 1–13.
[29] M. Langelaar, Topology optimization of 3d self-supporting structures for additive manufacturing, Addit. Manuf. 12 (2016) 60–70.
[30] M. Langelaar, Combined optimization of part topology, support structure layout and build orientation for additive manufacturing, Struct. Multidiscip. Optim. 57 (5) (2018) 1985–2004.
[31] M. Leary, L. Merli, F. Torti, M. Mazur, M. Brandt, Optimal topology for additive manufacture: a method for enabling additive manufacture of support-free optimal structures, Mater. Des. 63 (2014) 678–690.
[32] J. Liu, A.T. Gaynor, S. Chen, Z. Kang, K. Suresh, A. Takezawa, L. Li, J. Kato, J. Tang, C.C. Wang, et al., Current and future trends in topology optimization for additive manufacturing, Struct. Multidiscip. Optim. 57 (6) (2018) 2457–2483.
[33] A.M. Mirzendehdel, M. Behandish, S. Nelaturi, Topology optimization with accessibility constraint for multi-axis machining, arXiv:2002.07627 [abs], 2020.
[34] A.M. Mirzendehdel, K. Suresh, Support structure constrained topology optimization for additive manufacturing, Comput. Aided Des. 81 (2016) 1–13.
[35] J. Nocedal, S.J. Wright, Numerical Optimization, 2nd ed., Springer, 2006.
[36] S. Osher, J.A. Sethian, Fronts propagating with curvature-dependent speed: algorithms based on hamilton-jacobi formulations, J. Comput. Phys. 79 (1) (1988) 12–49.
[37] J. Sethian, Level Set Methods and Fast Marching Methods: Evolving Interfaces in Computational Geometry Fluid Mechanics, Computer Vision, and Materials Science, Cambridge University Press, 1999.
[38] O. Sigmund, Manufacturing tolerant topology optimization, Acta Mech. Sin. 25 (2) (2009) 227–239.
[39] G. Strano, L. Hao, R.M. Everson, K.E. Evans, A new approach to the design and optimisation of support structures in additive manufacturing, Int. J. Adv. Manuf. Technol. 66 (9) (Jun 2013) 1247–1254.
[40] E. van de Ven, C. Ayas, M. Langelaar, R. Maas, F. van Keulen, Continuous front propagation-based overhang control for topology optimization with additive manufacturing, Struct. Multidiscip. Optim. 57 (2018) 2075–2091.
[41] E. van de Ven, C. Ayas, M. Langelaar, R. Maas, F. van Keulen, Accessibility of support structures in topology optimization for additive manufacturing, Int. J. Numer. Methods Eng. 122 (8) (2021) 2038–2056.